

Review

Nonisothermal Crystallization Kinetics by DSC: Practical Overview

Sergey Vyazovkin ^{1,*}  and Nicolas Sbirrazzuoli ^{2,*} 

¹ Department of Chemistry, University of Alabama at Birmingham, 901 S. 14th Street, Birmingham, AL 35294, USA

² Institute of Chemistry of Nice, University Côte d'Azur, UMR CNRS 7272, 06100 Nice, France

* Correspondence: vyazovkin@uab.edu (S.V.); nicolas.sbirrazzuoli@univ-cotedazur.fr (N.S.)

Abstract: Providing a minimum of theory, this review focuses on practical aspects of analyzing the kinetics of nonisothermal crystallization as measured with differential scanning calorimetry (DSC). It is noted that kinetic analysis is dominated by approaches based on the Avrami and Arrhenius equations. Crystallization kinetics should not be considered synonymous with the Avrami model, whose nonisothermal applications are subject to very restrictive assumptions. The Arrhenius equation can serve only as a narrow temperature range approximation of the actual bell-shaped temperature dependence of the crystallization rate. Tests of the applicability of both equations are discussed. Most traditional kinetic methods tend to offer very unsophisticated treatments, limited only to either glass or melt crystallization. Differential or flexible integral isoconversional methods are applicable to both glass and melt crystallization because they can accurately approximate the temperature dependence of the crystallization rate with a series of the Arrhenius equations, each of which corresponds to its own narrow temperature interval. The resulting temperature dependence of the isoconversional activation energy can be parameterized in terms of the Turnbull–Fisher or Hoffman–Lauritzen theories, and the parameters obtained can be meaningfully interpreted and used for kinetic simulations.

Keywords: calorimetry; crystallization; glass; kinetics; melt; nonisothermal



Citation: Vyazovkin, S.; Sbirrazzuoli, N. Nonisothermal Crystallization Kinetics by DSC: Practical Overview. *Processes* **2023**, *11*, 1438. <https://doi.org/10.3390/pr11051438>

Academic Editor: Monika Wawrzekiewicz

Received: 13 April 2023

Revised: 1 May 2023

Accepted: 6 May 2023

Published: 9 May 2023



Copyright: © 2023 by the authors. Licensee MDPI, Basel, Switzerland. This article is an open access article distributed under the terms and conditions of the Creative Commons Attribution (CC BY) license (<https://creativecommons.org/licenses/by/4.0/>).

1. Introduction

Crystallization typically generates substantial amounts of heat that can be monitored calorimetrically. This makes the technique of differential scanning calorimetry (DSC) a major tool in crystallization studies. The Scopus database lists close to 37,000 publications associated with the application of calorimetry to the process of crystallization [1]. More than 20% of these publications deal with kinetics. Currently, the absolute majority of crystallization kinetic studies are performed under nonisothermal conditions. In spite of persistent research interest, the topic of the kinetic methodology of analyzing DSC data on nonisothermal crystallization kinetics has not been a subject of a systematic review for over 20 years. Although many aspects of the early review articles [2–4] continue to remain relevant, significant progress has been made in the methodology of nonisothermal kinetics of simple [5] and complex [6] processes, including crystallization. In particular, more accurate and efficient methods have been developed, whereas certain widespread methods reviewed earlier [2–4] have been found to be inadequate or downright faulty. Moreover, the previous reviews present only a particular perspective limited to the crystallization of either low molecular weight glasses [2,3] or macromolecular melts [4], so the techniques surveyed tend to be specific to either heating or cooling conditions.

The present review endeavors to highlight approaches that are equally applicable for treating the crystallization kinetics taking place on cooling as well as on heating. While giving a minimum of theory, it focuses on practical aspects of proper kinetic analysis that can be accomplished by a variety of contemporary and traditional methods. It is hoped that this review will be of interest and value to the broad community of researchers intent

on advancing their understanding of the nonisothermal crystallization kinetics of materials with the aid of DSC.

2. Some Basics

The heat flow measured with DSC is proportional to the process rate. It is almost universally accepted that the proportionality is linear, i.e.,:

$$\frac{d\alpha}{dt} = \frac{1}{Q_0} \frac{dQ}{dt} \quad (1)$$

where α is the extent of conversion from the initial to the final state, t is the time, dQ/dt is the heat flow, Q_0 is the total heat released or absorbed during conversion. In fact, the linear proportionality results from a simplifying assumption introduced originally by Borchardt and Daniels [7]. They assumed that the so-called thermal inertia term could be neglected in the heat flow equation. However, this assumption may not hold under certain experimental conditions and, thus, have a detrimental effect on kinetic evaluations [8,9]. Note that some early crystallization kinetics studies were conducted with an account of thermal inertia [10].

Generally, the raw heat flow (RHF) signal, i.e., a DSC peak uncorrected for thermal inertia, is shifted to some degree to a higher temperature. This temperature shift is eliminated by adjusting RHF as follows:

$$\frac{dQ}{dt} = RHF + \tau \frac{d(RHF)}{dt} \quad (2)$$

where the second term on the right-hand side is the thermal inertia term (Figure 1). The time constant, τ , is readily determined from a DSC peak for the melting of a pure metal [11]. The magnitude of the temperature shift can be estimated as $\beta\tau$, where β is the heating rate.

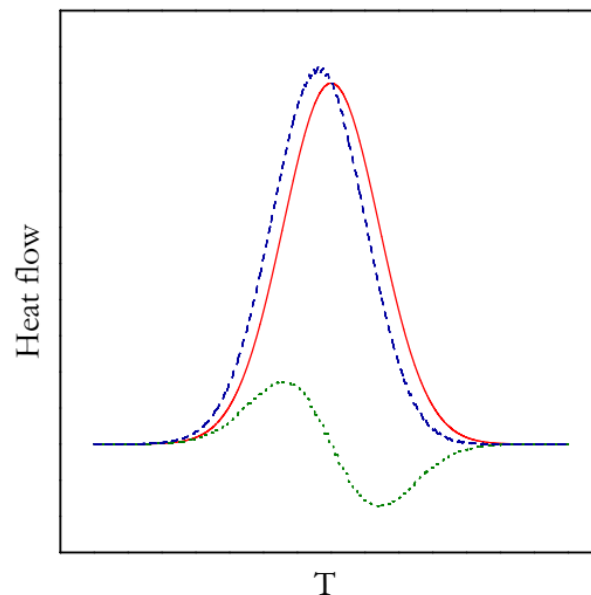


Figure 1. Schematic illustration of the thermal inertia effect. Uncorrected (solid line) and corrected (dashed line) DSC peaks. Thermal inertia term (dotted line).

Because τ is proportional to the total heat capacity and, thus, the sample mass, the effect of thermal inertia is diminished by conducting DSC measurements on smaller masses and at slower heating rates. However, such conditions may not be suitable for low enthalpy processes. By way of example, recrystallization of copper releases only 1 J/g of heat, so the process has to be measured on a rather heavy 200 mg sample and at fast heating rates (2–80 K/min) [12]. The respective time constant is 17 s, which means that at 80 K/min, the temperature shift (i.e., $\beta\tau$) should be about 23 K. In such a situation, one must obviously

make a correction (Equation (2)) for thermal inertia. Remarkably, the use of the raw data yields an activation energy estimate of 98 kJ/mol, whereas adjusting the data via an additional calibration [12] and correction for thermal inertia causes the activation energy to increase by 34% to 131 kJ/mol [9]. The importance of the thermal inertia effect in the case of large τ values is discussed in detail elsewhere [13,14].

On the other hand, for a 3 mg sample of isotactic polystyrene, τ is only 4 s, so at the fastest heating rate of 20 K/min, the temperature shift is just a little over 1 K [9]. Then, the correction for thermal inertia causes the activation energy to rise by less than 3%, which is less than the experimental uncertainty of the respective estimate. In this situation, the effect of thermal inertia can be considered negligible. It should normally be negligible as long as $\beta\tau$ does not exceed 2–3 K [9]. It must be stressed that using smaller masses and slower heating rates is generally a good approach because it minimizes the deviation between the programmed and actual sample temperature, which is critical for reliable kinetic calculations. Acceptable heating rates and masses differ depending on the process enthalpy and thermal conductivity [15,16]. For crystallizations, one rarely needs masses heavier than 10 mg and heating rates faster than 20 K/min. Perhaps the simplest advice is to select conditions such that the DSC heat flow signal does not exceed 8 mW [17] which corresponds approximately to a 0.5 K [18] deviation between the programmed and actual sample temperature.

Subject to the proper measurement conditions, DSC provides data on the overall crystallization rate, which can be utilized for adequate kinetics analysis. Its starting point usually is parameterizing the rate via two variables: temperature (T) and conversion (α):

$$\frac{d\alpha}{dt} = k(T)f(\alpha) \quad (3)$$

The conversion is determined as the ratio of the partial and total areas of a DSC peak. In the case of crystallization, the conversion represents the relative degree of crystallinity. The word “relative” is used to emphasize the fact that many substances, especially polymers, do not crystallize completely. The temperature and conversion dependencies of the rate are described, respectively, by the rate constant, $k(T)$ and the reaction model, $f(\alpha)$. Oftentimes, Equation (3) is more convenient to use in its integral form:

$$g(\alpha) = \int_0^\alpha \frac{d\alpha}{f(\alpha)} = \int_0^t k(T)dt \quad (4)$$

The conversion dependence of the crystallization rate is most commonly described by the Avrami model. The model is sometimes called the Johnson–Mehl–Avrami–Erofeev–Kolmogorov [19–22] model to reflect the independent contributions of several scholars to its development. A concise overview of the theory behind the Avrami model is available elsewhere [23–26]. One of its commonly used mathematical forms is as follows:

$$g(\alpha) = [-\ln(1 - \alpha)]^{1/m} = \int_0^t k(T)dt \quad (5)$$

where m is the Avrami exponent.

Theoretically, the value of m is linked to the dimensionality of the crystal growth. However, this link is not straightforward, as it depends on the conditions of nucleation and growth [25]. For the same growth dimensionality, the Avrami exponent is larger by 1 for the steady state than for instantaneous nucleation. Additionally, relative to the surface-controlled growth, the m values for the growth controlled by diffusion are smaller and can be fractional. For instance, for the three-dimensional growth, m is 4 (steady-state nucleation, surface-controlled growth), 3 (instantaneous nucleation, surface-controlled growth), 2.5 (steady-state nucleation, diffusion-controlled growth), and 1.5 (instantaneous nucleation, diffusion-controlled growth). In all, the theoretically justified m values span the range from 0.5 to 6 [25]. ($m > 4$ is expected for sheaf-like growth per analysis by

Morgan [27]), so experimentally determining some value of m from that range cannot be directly interpreted in terms of the dimensionality without additional supporting evidence.

The most common description of the temperature dependence is by means of the Arrhenius equation:

$$k(T) = A \exp\left(\frac{-E}{RT}\right) \quad (6)$$

where A is the preexponential factor, E is the activation energy, and R is the gas constant. It is noteworthy that in crystallization kinetics, the Arrhenius equation is seen as a convenient approximation of the actual temperature dependence. A more accurate form of the latter can be presented by the Vogel–Tammann–Fulcher (VTF) equation by analogy with the temperature dependence of viscosity [2,3]. However, as shown in an early review [3], this type of dependence did not gain universal acceptance in crystallization kinetics. Up to this day, the Arrhenius form continues to be used most commonly.

Equation (5) can be differentiated with respect to time to obtain the rate (i.e., differential) equation. The latter, however, takes a cumbersome form [3] for nonisothermal conditions because T and, therefore, $k(T)$ become a function of t . If temperature is changed with time at a constant rate, β :

$$\beta = \frac{dT}{dt} \quad (7)$$

Equation (5) takes the following form:

$$[-\ln(1 - \alpha)]^{1/m} = \frac{A}{\beta} \int_{T_0}^T \exp\left(\frac{-E}{RT}\right) dT \quad (8)$$

Equation (8) is, at least in principle, applicable to either heating or cooling, i.e., to the crystallization of either glasses or melts. The left-hand side of Equation (8) is invariably positive. For cooling, the temperature integral turns negative because $T_0 > T$. Yet, the right-hand side remains positive because $\beta < 0$.

Since the temperature integral in Equation (8) cannot be solved analytically, it is commonly replaced with approximations of the following type:

$$[-\ln(1 - \alpha)]^{1/m} = \frac{A}{\beta} \int_0^T \exp\left(\frac{-E}{RT}\right) dT = \frac{AE}{\beta R} p(x) \quad (9)$$

where $x = E/RT$, and $p(x)$ is an approximating function [28]. This type of approximation replaces the lower integration limit in Equation (8) with zero. This is done to streamline integration with the aim of obtaining simple equations for parameterizing the process rate. Without going into unnecessary technical details, it is easy to arrive at an approximately linear equation of this kind [29–33]:

$$\ln[-\ln(1 - \alpha)] \cong C - \gamma \frac{mE}{RT} \quad (10)$$

where C is the temperature-independent constant containing the pre-exponential factor, and γ is a constant that, depending on $p(x)$, is either equal or nearly equal to 1.

Knowing the kinetic triplet (i.e., m , A , and E) allows one to simulate the overall crystallization kinetics under desired temperature conditions. It is, for example, of practical importance to be capable of simulating the so-called time-temperature-transformation (T-T-T) and temperature-heating rate-transformation (T-HR-T) diagrams [34,35]. In essence, a T-T-T diagram is a set of plots of t vs. T related to specific values of α . They are simulated with Equation (11):

$$t_\alpha = \frac{[-\ln(1 - \alpha)]^{1/m}}{A \exp\left(\frac{-E}{RT}\right)} \quad (11)$$

which is arrived at by integrating and rearranging Equation (5) for isothermal conditions. In it, t_α is the time to reach a specific conversion. By plugging a selected value of α and the estimated kinetic triplet into Equation (11) and then varying T , one obtains a t_α vs. T plot.

A T-HR-T diagram is a set of T_α vs. β plots corresponding to the selected α values. It is built by employing Equation (9). Again, one plugs a selected value of α and the estimated kinetic triplet into Equation (9). Then, β is varied in steps, finding at each step the upper integration limit T_α that secures the equality of the left- and right-hand sides of Equation (9). As a result, T_α vs. β plots are obtained. Successful examples of the simulated T-HR-T and T-T-T diagrams are found elsewhere [35–37].

3. Avrami–Arrhenius Treatment for Limited Temperature Range

The applications of the Avrami model are limited to the process of primary crystallization, i.e., the formation and growth of the crystallites until they spread throughout the space of the original noncrystalline phase. In turn, the crystallites can involve disordered or poorly ordered phases capable of further, i.e., secondary, crystallization. It is worth mentioning that there is a possibility to incorporate secondary crystallization into the Avrami model [38].

Speaking of the Avrami model limitations specific to nonisothermal conditions, they are discussed at length elsewhere [2,3,39]. Briefly, they arise from the fact that the Avrami equation results from the integration of the nucleation and growth rates under isothermal conditions. Under such conditions, the temperature dependencies of those rates can be combined into a single constant parameter, i.e., $k(T)$ in Equation (5). When temperature varies continuously, this creates a problem because both rates are temperature-dependent, and the corresponding dependencies generally are quite different. This limits the nonisothermal application of the Avrami model to two specific situations.

The first one was identified by Avrami as an isokinetic temperature range, which is the range where the ratio of the growth and nucleation rates remains constant [40]. Basically, it means that both rates have the same temperature dependencies or, simply, the same Arrhenius activation energy. This situation is explored by Farjas and Roura [32], who find that the inequality of the activation energies gives rise to a constant multiplier in Equation (8), which remains valid.

The second situation is known as site saturation, which occurs when a system becomes saturated with nuclei at the early stages of crystallization [3,39,41]. Then, the rate of crystallization becomes limited by the nuclei growth. This permits reducing the temperature dependence of the crystallization rate to that of the growth that is assumed to be Arrhenian.

It is noteworthy that the problems associated with the Avrami model have received much more attention than those related to the use of the Arrhenius equation. There is no doubt that the temperature dependence of the crystallization rate is not Arrhenian [42]. Actual forms of the dependence are discussed briefly in the next sections. For now, we only mention that a non-Arrhenian behavior of the dependence is readily detectable when the crystallization kinetics is studied in a sufficiently broad temperature range. An example of such a study is presented in Figure 2 [43]. This is melt and glass crystallization of poly(trimethylene terephthalate) conducted under isothermal conditions [44]. Fitting the Avrami model has produced the rate constants at each temperature. The results are presented as an Arrhenius plot, $\ln k(T)$ vs. $1/T$, which, according to Equation (6), is supposed to be linear. The distinct nonlinearity of the resulting plot becomes unmistakably detectable as the temperature range approaches 20 K (Figure 2). It is also seen that as the temperature rises, the slope of the plot is continuously changing, turning its value from negative to positive. Respectively, the corresponding value of E decreases with increasing temperature, turning its value from positive (glass crystallization) to negative (melt crystallization). This means that in the latter case, the temperature dependence becomes anti-Arrhenian.

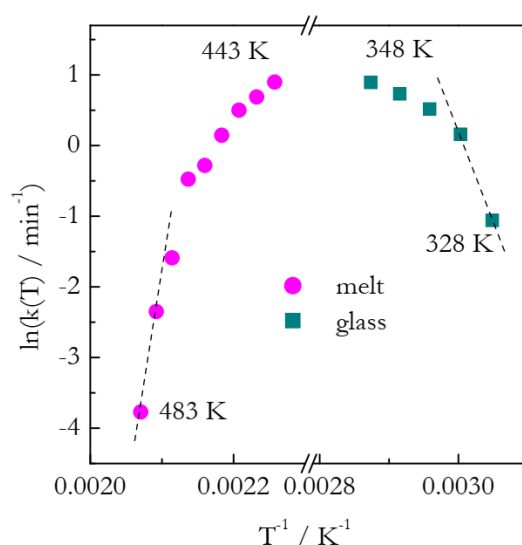


Figure 2. Arrhenius plot for glass (squares) and melt (circles) crystallization of poly(trimethylene terephthalate). Crystallization temperature ranges: 328–348 K (glass); 443–483 K (melt). Data from Hong et al. [44]. Dashed line is a guide to the eye to better visualize nonlinearity. Adapted with permission from Vyazovkin [43]. Copyright 2015 Springer.

Overall, the Arrhenius equation is no more than a convenient approximation that can hold for a relatively narrow temperature range, apparently less than 20 K. In nonisothermal crystallization studies, the temperature ranges covered tend to be broader. Normally, the width of a crystallization DSC peak is no less than 30–40 K. Whether the Arrhenius approximation holds can and should be tested by checking the experimentally determined activation energy for constancy, as discussed further.

Relatedly, before applying the Avrami model, it is critical to test whether it is applicable to the crystallization under study. Simply fitting data and finding that the fit is characterized by a statistically significant correlation coefficient (or other statistical criteria) is a necessary but not sufficient condition of applicability. The Avrami model is known to be flexible enough to imitate other solid-state reaction models [45]. For instance, it can fit near perfectly a process following the Jander diffusion model in the α range of about 0–0.8 [30].

Malek [46] has proposed a rather definitive criterion based on the position of the maximum of the $z(\alpha)$ function:

$$z(\alpha) = \frac{d\alpha}{dt} T^2 \quad (12)$$

This function is readily obtained from experimentally measured DSC curves and should be nearly identical at different heating rates. Regardless of the Avrami exponent value, the $z(\alpha)$ function should have a maximum at $\alpha = 0.632 \pm 0.02$ [46]. Svoboda has argued that the application of the Avrami model can still be justified if the $z(\alpha)$ maximum is found in a broader range of α [47].

If the Avrami model is found inapplicable, a viable alternative is to employ the general autocatalytic model:

$$f(\alpha) = \alpha^M (1 - \alpha)^N \quad (13)$$

which is also known as the extended Prout–Tompkins or truncated Sestak–Berggren model [5]. The advantage of this model is two-fold. First, the Avrami models having different m values can be almost perfectly represented by certain combinations of M and N in Equation (13) [48,49]. In principle, a combination of the M and N values can be used to identify a variety of solid-state reaction models [49]. Second, Equation (13) is still applicable when the crystallization kinetic curve is not of sigmoid type. Such is an example of zero-order kinetics that is apparently associated with surface crystallization [50,51]. The situation is analogous to the zero-order kinetics encountered in other surface-limited

processes, such as the vaporization of liquids [52], solid-state polymerization [53], and certain topochemical reactions of solids [54].

When the Avrami model is applicable, one can employ Equation (10) (or similar) for estimating the kinetic parameters. One problem to notice, though, is that plotting $\ln[-\ln(1 - \alpha)]$ against $1/T$ yields m and E in a conjoint form, i.e., as a single combined parameter mE . It may seem that this problem can be resolved by dividing both sides of Equation (10) by m , which results in a plot whose slope is E . That is, by varying m , one might possibly find m and E individually as the values corresponding to the best statistical fit. Nevertheless, this approach fails when the fitting is performed on the data obtained at a single heating rate.

A remarkable example of such failure is provided by Perez–Maqueda et al. [55], who demonstrate that simulated data ($m = 2$) can be fitted equally well (correlation coefficient equals 1) by a set of the Avrami models having m from 1.5 to 4. The respective Arrhenius parameters vary over a wide range falling on a straight line (Figure 3). The essence of this effect, also known as the compensation effect, is that estimating an incorrect value of E is compensated by estimating an incorrect value of $\ln A$ in such a way that the respective $k(T)$ value in the middle of the experimental temperature range remains practically unaffected [56]. This is the primary reason why several models with widely differing Arrhenius parameters can satisfactorily describe the same set of experimental data.

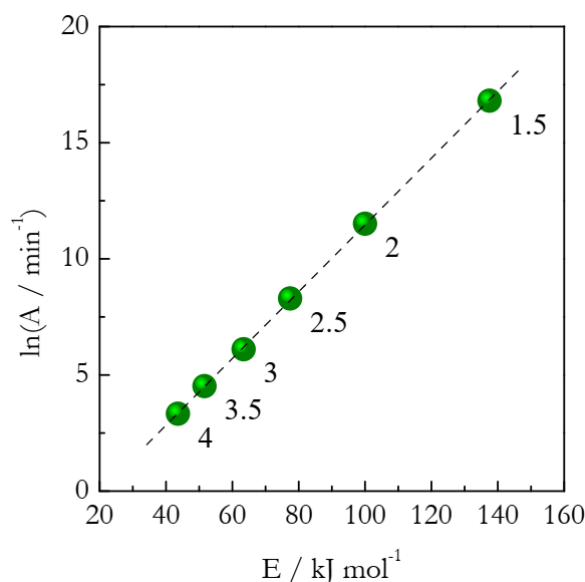


Figure 3. Uncertainty in the Arrhenius parameters resulting from selecting various values of m to fit single heating rate data simulated for $m = 2$, $E = 100 \text{ kJ/mol}$, and $A = 10^5 \text{ min}^{-1}$. Numbers by the points are the Avrami exponent values. Data from Perez–Maqueda et al. [55].

Nonetheless, no such failure occurs when the fitting is performed by simultaneously employing the datasets obtained at several heating rates. Indeed, in this situation, fitting the Avrami model results in uniquely retrieving the correct kinetic triplet [55]. This example reinforces the recommendation of the International Confederation for Thermal Analysis and Calorimetry (ICTAC) that single heating rate methods should be avoided in favor of methods that use multiple heating rates simultaneously [5]. Ignoring this simple recommendation leads to estimating invalid kinetic triplets, which, when used in simulations, produce entirely meaningless results [57,58].

As already mentioned, fitting Equation (10) to crystallization data yields the conjoint parameter mE . It can be separated into its components using the methods that afford estimating either m or E individually. The Avrami exponent can be determined directly with the aid of the classical method by Ozawa [59]. The method does not assume any particular temperature dependence for the crystallization process. Rather, it avoids the

issue by using isothermal cuts through the nonisothermal data. Then, the m value is estimated from Equation (14).

$$\ln[-\ln(1-\alpha)] = \text{Const} - m \ln \beta \quad (14)$$

as the slope of a linear plot of the left-hand side against $\ln \beta$. In Equation (14), the α values are the conversions corresponding to a selected temperature but at different β 's. The equation holds for both heating and cooling, i.e., glass and melt crystallization.

A disadvantage of the Ozawa plot is that it usually has very few points, i.e., at most, as many as the number of the heating or cooling rates used. This is illustrated in Figure 4 for the melt and glass crystallization of poly(ethylene 2,5-furandicarboxylate) (PEF) [60].

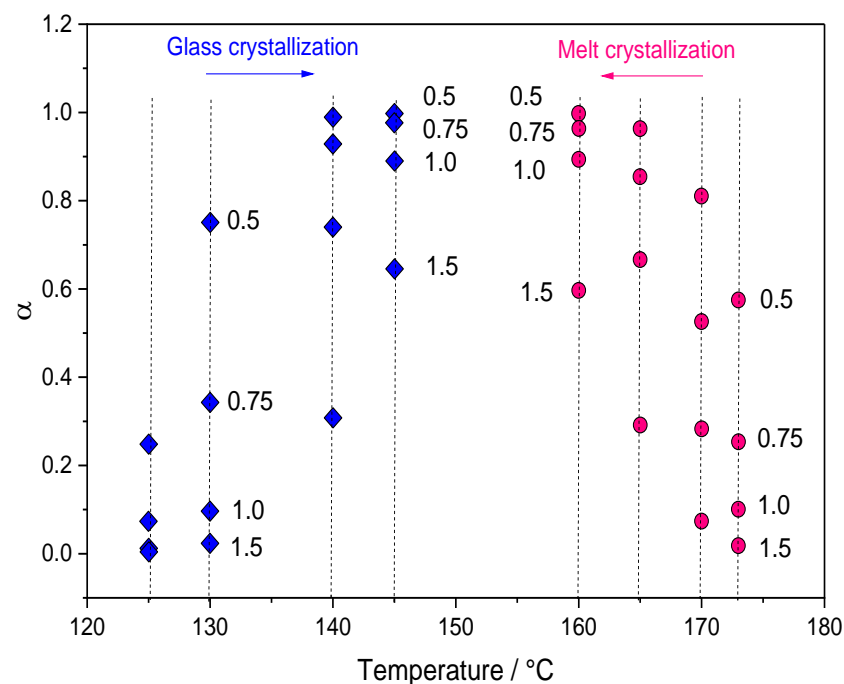


Figure 4. Data needed for constructing the Ozawa plots, i.e., α values reached at different β 's for several selected temperatures. Data collected for crystallization of PEF at four heating/cooling rates (0.5, 0.75, 1.0, and 1.5 K min⁻¹). Adapted with permission from Codou et al. [60]. Copyright © 2014 Wiley-VCH.

It is seen that as the temperature approaches the limits of the experimental range, the range of α narrows so that the use of either the fastest or slowest rates of heating/cooling becomes practically impossible. This disadvantage is overcome in a recent modification of the method by Toda [61,62]. It permits obtaining modified Ozawa plots that have as many points as the number of points on an experimentally measured α vs. T curve.

When it comes to estimating m , there is a popular misconception that it can be performed by substituting nonisothermal data in the isothermal form of the Avrami equation:

$$\ln[-\ln(1-\alpha)] = m \ln k(T) + m \ln t \quad (15)$$

Equation (15) is obtained by integrating Equation (5) at $T = \text{const}$. The erroneous idea is that the time in Equation (15) can be determined from nonisothermal data by using Equation (7). That is, for heating:

$$t = \frac{T - T_0}{\beta} \quad (16)$$

where T_0 is the temperature at which crystallization starts, and β is the heating rate. A similar expression is easily obtained for cooling. The fallacy of such an approach is quite

obvious; Equation (15) is undoubtedly isothermal, whereas each value of t determined from Equation (16) corresponds to a different temperature. Unfortunately, this approach is the essence of a popular method by Jeziorny [63]. A failure of the method to determine the correct values of m is well demonstrated for simulated [64] and experimental data [65]. A recent theoretical analysis of the method shows [33] that for nonisothermal data, the slope of the Avrami plot $\ln[-\ln(1 - \alpha)]$ vs. $\ln t$ does not yield the expected value of m . Instead, the value of the slope has a rather complex form [33]:

$$\frac{d \ln[-\ln(1 - \alpha)]}{d \ln t} = 1.92m \frac{\beta t}{T_0 + \beta t} + 1.0008m \frac{E}{R} \frac{\beta t}{(T_0 + \beta t)^2} \quad (17)$$

Furthermore, Equation (17) indicates that, typically, the slope value should significantly exceed the correct m values [33]. This inference is consistent with previous reports [61,64,65]. Clearly, neither the Jeziorny method nor any other approach based on combining Equations (15) and (16) should be used in kinetic analysis of nonisothermal crystallization.

Not only m but also E can be determined individually. This is done routinely with the help of isoconversional methods [5,43,66]. The most straightforward isoconversional method is that of Friedman [67]. Its equation:

$$\ln\left(\frac{d\alpha}{dt}\right)_\alpha = \ln[A_\alpha f(\alpha)] - \frac{E_\alpha}{RT_\alpha} \quad (18)$$

is obtained directly by combining Equations (3) and (6). Henceforth, the subscript α denotes the values related to a specific value of conversion. The method does not require any assumptions about the reaction model $f(\alpha)$ as it affords estimating the activation energy directly from the slope of the linear plot of the natural logarithm of the rate vs. reciprocal temperature. Naturally, both of these values should correspond to the same conversion at different heating or cooling rates, β .

Isoconversional methods allow one to test whether the Arrhenius approximation holds. This is accomplished by checking the constancy of the isoconversional activation energy, E_α . Isoconversional methods yield E_α as a function of α in a broad range of conversions. Usually, less than 10% variability in E_α within the α range 0.1–0.9 [6] or 0.3–0.7 [46] is judged as acceptable constancy.

An instructive example is displayed in Figure 5, which shows the E_α dependencies for two DSC crystallization peaks, which occur during the crystallization of $\text{Si}_{12.5}\text{Te}_{87.5}$ glass [68]. Clearly, for the first peak, E_α is practically constant and, therefore, can be replaced with a single average value. Nevertheless, for the second peak, the variability in E_α exceeds either of the above criteria, so one cannot replace E_α with the mean value. This complicates further kinetic analysis, some options of which are discussed later.

If E_α is deemed reasonably constant, one can safely use the previously mentioned methods for estimating the kinetic triplet. One should also be aware of a number of other time-proven methods recommended by ICTAC [5].

It is important to notice that the differential isoconversional method of Friedman is applicable to the data obtained on heating as well as on cooling. In other words, it can be used for the crystallization of glasses as well as of melts. As far as integral isoconversional methods, they may or may not be applicable to the processes conducted on cooling. The applicability depends on the manner of integration, which can be characterized as either rigid or flexible [43,66].

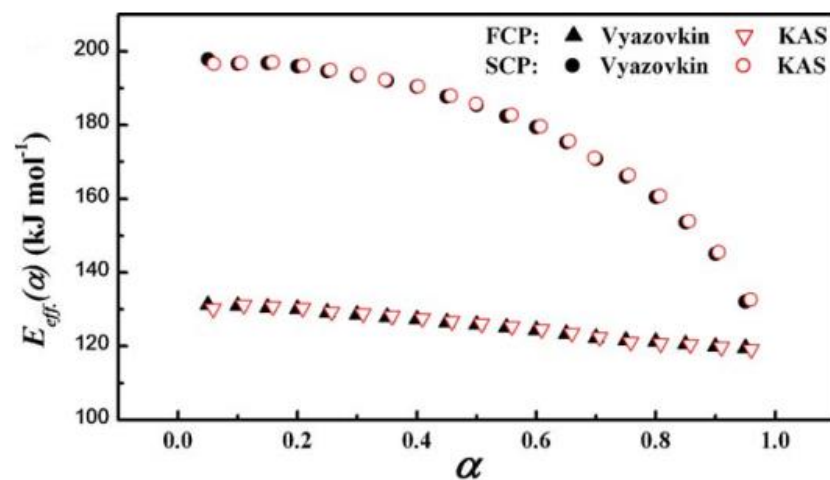


Figure 5. Variations of isoconversional activation energy E_{α} estimated by two methods (Vyazovkin and Kissinger–Akahira–Sunose) for crystallization of $\text{Si}_{12.5}\text{Te}_{87.5}$ glass. FCP and SCP stand for the first and second DSC crystallization peaks. Reproduced with permission from Abu El-Oyoun [68]. Copyright 2011 Elsevier.

Some integral methods are derived via integration from 0 to T (c.f., Equation (9)), which gives rise to equations that contain only one temperature (the upper limit of integration). This means that the equations of such methods are obtained with integration for the conditions of heating that are built into these methods in a rigid manner, i.e., it cannot be changed. Other integral methods are derived with integration between two temperature limits (c.f., Equation (8)) which makes these methods flexible because the limits can be changed in a flexible manner. In the flexible methods, integration can be performed from lower to higher as well as from higher to lower temperature, which corresponds, respectively, to heating and cooling. Nevertheless, the most popular integral methods (Ozawa [69], Flynn–Wall [70,71], Kissinger–Akahira–Sunose [72], Starink [73]) are rigid and, thus, cannot be used to study the kinetics on cooling. The same applies to Equation (10). Unfortunately, this crucial issue never comes up in the early reviews [2,3], perhaps because they focus only on the crystallization of glasses, which occurs on heating.

On the other hand, the flexible isoconversional methods are entirely suitable for kinetic studies on both heating and cooling. Among about a dozen of the flexible methods [6,43,66], those by Vyazovkin [74] and Ortega [75] are probably used most commonly.

In addition, one should bear in mind that the rigid methods introduce a systematic error in the E_{α} value when it varies with α . The error increases with the magnitude of variation and can easily reach 20% [76]. The error does not occur in the flexible integral methods, and, of course, it does not appear in the differential method of Friedman. Related to that error is the issue of the concurrent use of several isoconversional methods. Typically, they tend to produce the E_{α} dependencies that are qualitatively similar, e.g., E_{α} that decreases with α regardless of the method used. The dependencies will also usually be almost identical quantitatively when one applies several rigid methods concurrently. This is sometimes mistakenly taken as a sign of the validity of the obtained E_{α} dependencies. In reality, this is only a sign that the $p(x)$ approximations (Equation (9)) used by these methods have very similar accuracy. That is why the ICTAC recommendations [5] advocate avoiding concurrent use in favor of using one of the most accurate methods. The latter include the flexible integral as well as differential methods. When the E_{α} dependence evaluated by such methods is compared to the dependence evaluated by a rigid method, the two dependencies are likely to manifest qualitative similarities but reveal significant quantitative differences. This difference becomes critical when the E_{α} dependence is employed for further numerical evaluations, examples of which are discussed in Sections 4 and 5.

Some comments must also be made regarding the use of the Kissinger method [77], the basic equation of which is:

$$E = -R \frac{d \ln \left(\frac{\beta}{T_p^2} \right)}{dT_p^{-1}} \quad (19)$$

where T_p is the temperature that corresponds to the rate peak maximum. T_p is easily determined as the DSC peak temperature. Then, E is found as the slope of the plot of $\ln \left(\frac{\beta}{T_p^2} \right)$ vs. T_p^{-1} . While being extremely popular, the method has multiple shortcomings, as discussed at length in a recent review paper [78]. To avoid unnecessary repetitions, we only bring up two issues that are most critical for the process of crystallization.

First, the method cannot be applied to the data obtained on cooling [79]. That is, it should never be used to study the melt crystallization kinetics. Alas, the earlier review [4] suggests the Kissinger method as a possible way of estimating the activation energy from cooling data. In fact, forcing the method to treat data obtained on cooling yields entirely erroneous values of E [79,80]. It must be stressed that a similar conclusion is reached by Shi et al. [81] regarding the method of Matusita and Sakka [82], which is a close analog of the Kissinger method.

Second, unlike isoconversional methods, the Kissinger method is not well suited for testing whether the Arrhenius approximation holds. If it does not, the Kissinger plot should, in principle, become nonlinear. However, such nonlinearity is difficult to detect, even when an isoconversional method demonstrates obvious variability in E_α [78]. An example relevant to crystallization is shown in Figure 6. This is the crystallization of poly(ethylene 2,6-naphthalate) (PEN) glass measured with DSC at five heating rates from the range of 5–15 K/min [83]. It is seen that E_α demonstrates a significant variability. However, the Kissinger plot reveals no obvious signs of nonlinearity. The latter is likely masked by the natural scatter in the experimental T_p values. Usually, one has a better chance to detect the Kissinger plot nonlinearity when using more heating rates from a broader range.

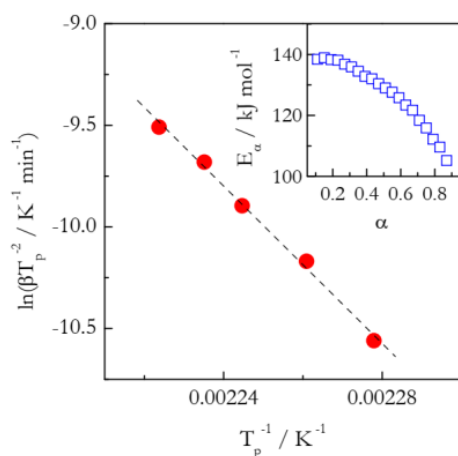


Figure 6. Crystallization of PEN glass. Kissinger plot demonstrates statistically significant linearity ($r = -0.9977$). Inset shows variation in isoconversional activation energy. Adapted with permission from Vyazovkin and Dranca [83]. Copyright 2006 Wiley-VCH.

Finally, some discussion is due regarding kinetic analysis in the case when E_α is found to be significantly variable (c.f., Figures 5 and 6). Significant variation in E_α is a strong indicator of the process kinetics being driven by more than a single step. In practical terms, it means that the single-step kinetic analysis based on a combination of Equations (3) and (6) becomes unsound. Some alternative kinetic treatments should be used instead. The basic principles of such treatments are quite simple and applicable to

various kinds of processes, not only to crystallization [6]. It seems reasonable to accept the fact that a significant variability in E_α most commonly arises from the kinetics that face at least two energy barriers [84]. To date, there are two ways to account for this fact. The first is to maintain Equation (3) but replace the Arrhenius temperature dependence in $k(T)$ with one appropriate for the crystallization kinetics. This approach is discussed in the next two sections.

The second way is to preserve the Arrhenius temperature dependence in $k(T)$ but use more than one rate Equation (3). In the field of crystallization, such an approach has been explored by the so-called “deconvolution” technique. As already pointed out [6], nowadays, this term is frequently applied to mean the procedure of resolving overlapped peaks, which differs from the original mathematical meaning of the term. The procedure is used in two variants: mathematical and kinetic deconvolution [6].

In mathematical deconvolution, overlapped rate peaks are separated into individual peaks by using some mathematical functions $F_i(t)$ as follows:

$$\frac{d\alpha}{dt} = \sum_{i=1}^N F_i(t) \quad (20)$$

where N is the number of individual peaks, and $F_i(t)$ is a function having the peak shape. For example, the Fraser–Suzuki function appears to have been employed most frequently. Conceptually, each separated peak is expected to represent an individual reaction step. Then, these individual steps are subjected to the regular single-step kinetic analysis as discussed above as well as elsewhere [5]. In particular, it is necessary to apply an isoconversional method to test the constancy of E_α , which would confirm that an individual, separated step is indeed a single step. If the constancy of E_α cannot be confirmed, it can also mean that the experimentally measured overall rate in Equation (20) cannot be represented as the sum of the rates related to several *independent* steps.

In kinetic deconvolution, overlapped rate peaks are resolved into separate peaks by employing a set of the rate Equation (3), i.e., in the following fashion:

$$\frac{d\alpha}{dt} = \sum_{i=1}^N c_i k_i(T) f_i(\alpha_i) \quad (21)$$

where c_i is the contribution (weight) of the i -th kinetic step. Although, per Equation (21), the overlapped rate peaks are separated into several single steps, it does not mean that each resulting individual peak necessarily represents single-step kinetics. This only has to happen when the experimentally measured overall rate in Equation (21) can be represented as the sum of the rates related to several *independent* steps. Thus, testing the constancy of E_α for each of the peaks is relevant.

Note that the multistep kinetic model implicit in Equations (20) and (21) is that of parallel *independent* reactions. It is valid when a system has at least two independent reaction centers. The simplest example is a mechanical mixture of two reactants or a single reactant that is complex enough to possess more than one reaction center. However, one must not forget that overlapped rate peaks also arise from consecutive steps. The consecutive steps are not independent, and their overall kinetics cannot be reduced to Equation (20) or Equation (21).

A systematic application of deconvolution in crystallization kinetics has been initiated by Svoboda and Malek [85], who carefully explored the use of the Fraser–Suzuki function. In particular, they succeeded in separating surface and bulk crystallization in the overall crystallization of a SeTe glass. Of particular interest is a discussion [86] of the pros and cons of mathematical and kinetic deconvolution. Regardless of the deconvolution type, one should be wary of the computational aspect of the procedure. Since the Fraser–Suzuki function has four fit parameters, one has to optimize eight of them in the simplest case of resolving two peaks. For the same case, the kinetic deconvolution based on the Avrami

model boils down to the optimization of six parameters, whereas the one based on the autocatalytic model to the optimization of eight. These are the types of computations that tend to converge to multiple local minima so that finding a unique and stable solution is a problem on its own [6].

According to Liland et al. [87], it appears that both types of deconvolution work reasonably well on partially overlapped peaks, whereas neither of them can adequately treat the kinetics that manifests themselves as fully overlapped peaks. In this regard, some promising results are obtained by utilizing artificial neural networks [87]. The first applications of this methodology in thermal analysis kinetics date back to an early work by Sbirrazzuoli et al. [88,89].

To conclude, it should be recognized that these days most crystallization kinetics analyses are conducted by means of the single-step Avrami–Arrhenius treatment. Unfortunately, this is commonly done without a proper justification. Namely, the Avrami model and single-step Arrhenius equation are employed without testing their applicability to a process under study. Even when tested, a significant dependence of $E\alpha$ on α is frequently ignored by replacing it with an average value in order to force unjustifiably oversimplified single-step treatment. The computational simplicity of such treatment oftentimes inspires inconsequential studies when a small set of DSC data is treated by several similar methods to redundantly generate multiple sets of the Avrami exponents and/or activation energies. Hopefully, the discussion presented in this and the following sections will help to hold back this type of unnecessary computational exercise in favor of physically meaningful kinetic analyses.

4. Turnbull–Fisher Treatment for Broad Temperature Range

As stated earlier, the temperature dependence of the crystallization rate is generally non-Arrhenian (Figure 2). In fact, in a broad temperature range, the rate of crystallization reveals a distinct maximum. This phenomenon has been known since at least the 1898 work by Tammann [90], who demonstrated the existence of such maxima for a series of organic compounds. Figure 7 presents Tammann’s data for the crystallization of molten piperine in a ~ 90 K temperature range. Since the data present the number of crystals formed for the same period of time (10 min), they can be interpreted as an estimate of the nucleation rate.

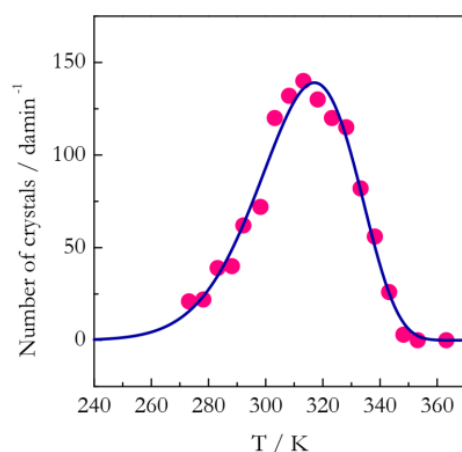


Figure 7. Crystallization of piperine melt at different temperatures. Points are the number of crystals formed in 10 min (i.e., in 1 damin) at each temperature. Data from Tammann [90]. Solid line is data fit with the Turnbull–Fisher model (Equation (22)).

The existence of such a rate maximum is well explained by the nucleation model of Turnbull and Fisher [91]:

$$n = n_0 \exp\left(\frac{-E_D}{RT}\right) \exp\left(\frac{-\Delta G^*}{RT}\right) \quad (22)$$

where n is the nucleation rate, n_0 is the preexponential factor, E_D is the activation energy of diffusion, and ΔG^* is the free energy barrier to nucleation. The model holds for a variety of nucleation-driven processes in the condensed phase.

In Equation (22), the E_D exponential term yields a regular Arrhenian temperature dependence, i.e., an exponential rate increase with increasing temperature. The maximum arises because the ΔG^* exponential term introduces an anti-Arrhenian dependence. For a spherical nucleus, ΔG^* is derived [23–25,43] as follows:

$$\Delta G^* = \frac{16\pi\sigma^3 T_m^2}{3(\Delta H_m)^2 (\Delta T)^2} = \frac{\Omega}{(\Delta T)^2} \quad (23)$$

where σ is the surface energy (surface tension), T_m is the equilibrium melting temperature, ΔH_m is the enthalpy of melting per unit volume, $\Delta T = T_m - T$ is the supercooling, and Ω includes all parameters that are practically independent of temperature.

Per Equation (23), lowering the temperature below T_m raises ΔT that makes the ΔG^* barrier progressively smaller. As a result, the rate accelerates with decreasing temperature, which constitutes an anti-Arrhenian temperature dependence. The product of the E_D and ΔG^* exponential terms (Equation (22)), i.e., of the Arrhenian and anti-Arrhenian dependencies, gives rise to a temperature dependence with a maximum (Figure 7).

When approximated by (i.e., fitted to) the Arrhenius equation, such dependence gives rise to the activation energy that changes its value and sign depending on temperature (Figure 8). Such variable activation energy is commonly termed as effective to emphasize the fact that its value does not necessarily identify with the energy barrier of a particular reaction step [84]. At small supercoolings, the nucleation rate is dominated by the ΔG^* exponential term; the temperature dependence is anti-Arrhenian, which leads to negative E values. The latter are routinely encountered when studying nucleation-driven processes such as crystallization, gelation, and morphological solid–solid transitions during continuous cooling [43,66,84].

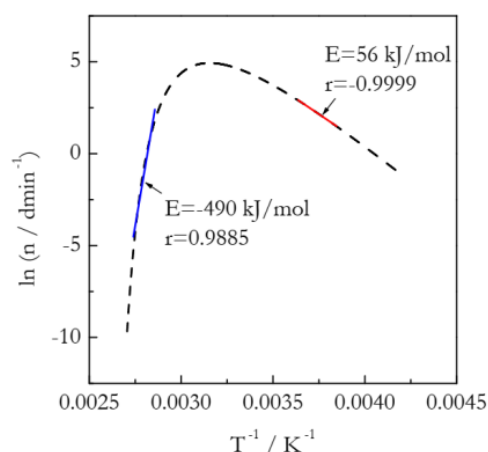


Figure 8. Turnbull–Fisher fit from Figure 7 cast as Arrhenius plot (dashed line). Solid lines are approximations by straight lines (Arrhenius equation with constant E) over two temperature intervals 15 K wide located at small (smaller T^{-1} values) and large (larger T^{-1} values) supercooling. E and r represent the respective Arrhenius activation energies and correlation coefficients.

Understandably, cooling by itself does not cause the effective activation energy to become negative. Performed on cooling, common chemical reactions, such as thermal decomposition and polymerization, maintain positive activation energies [92,93]. The negative activation energies for nucleation-driven processes are specific to the temperature region of small supercoolings (Figure 8). For crystallization, this region is normally accessible by cooling melted substances. On the other hand, the temperature region of large supercoolings is usually accessed by heating compounds from the glassy state. In

this region, the nucleation rate is dominated by the E_D exponential term. This is what makes the effective activation energies for the crystallization of glasses positive and of melts negative (Figure 8).

Upon making a simplifying assumption that at small supercoolings (i.e., in cooling DSC runs), the temperature dependence is determined only by the ΔG^* exponential term in Equation (22), one can determine the Ω value and, therefore, ΔG^* via Equation (23). For example, Clavaguera et al. [94] have demonstrated that it can be estimated from a Kissinger-like dependence:

$$\frac{d \ln \left(\beta (3T_p - T_m) / T_p^2 (T_m - T_p)^3 \right)}{d \left(1 / (T_p (T_m - T_p)^2) \right)} \approx -B \quad (24)$$

where B multiplied by R gives Ω . Alternatively, Sunol [95] proposed to determine B via linear isoconversional plots:

$$\left[\frac{\partial \ln(d\alpha/dt)}{\partial (T(\Delta T)^2)^{-1}} \right]_{\alpha} = -B_{\alpha} \quad (25)$$

Per Equation (25), one obtains a dependence of B_{α} on α . An advantage of such a method is that one can also test the constancy of B_{α} , which is expected based on Equation (23). Indeed, experimental values of B_{α} appear to show reasonable constancy [36,96]. Most importantly, both techniques allow one to simulate the time—cooling rate—transformation and TTT diagrams [36,94–96].

Similar evaluations can be carried out by using the method of Dobрева et al. [97,98]. It makes use of an equation, which is similar to Equation (22), but instead of ΔG^* , it employs the value of the work to create a nucleus. However, under iso-(thermal/baric) conditions, these two values are equal [99]. By virtue of the aforementioned simplifying assumption, the method derives the following linear plot for cooling DSC runs (i.e., small supercoolings):

$$\ln \beta = D - \frac{C}{\Delta T_p^2} \quad (26)$$

where D and C are parameters, and ΔT_p is determined from the DSC peak temperature as $T_m - T_p$. Note that Barandiaran and Colmenero [100] derived Equation (26) without specifying the meaning of the parameter C years before Dobрева et al. [97,98]. The latter, however, made its meaning clear. All things considered, C multiplied by RT_m should be equal to Ω .

Barandiaran and Colmenero have proposed to employ Equation (26) for estimating the so-called critical cooling rate, β_{cr} [100], i.e., the cooling rate, above which crystallization would be suppressed so that the melt would vitrify instead of crystallizing. Their idea is that β_{cr} can be estimated by Equation (26) as β corresponding to infinite supercooling, i.e., as follows:

$$\ln \beta_{cr} = D \quad (27)$$

On the other hand, Cabral et al. [101] argued that for a more accurate estimate, one should use Equation (28):

$$\ln \beta_{cr} = D - \frac{C}{T_m} \quad (28)$$

Equations (27) and (28) are compared for a series of inorganic systems and found to predict very similar β_{cr} values that tend to be markedly overestimated [101]. Similar conclusions are arrived at in another study of inorganic glasses [102]. Testing these equations on a series of organic pharmaceutical systems demonstrates that the predicted β_{cr} can be underestimated as well as overestimated [103].

Equation (26) is recommended [98] for estimating the nucleation activity of various additives. It is characterized as the ratio of the C values related to the nucleated and original material. It is naturally expected ΔG^* and, thus, C to be smaller for heterogeneous nucleation in the presence of an additive. The lower the ratio drops below 1, the higher the nucleation activity is. The $\ln\beta$ vs. ΔT_p^{-2} plots are sometimes found to be nonlinear, which complicates this type of analysis [104,105]. An example of such plots for the crystallization of polyethylene terephthalate (PET) is displayed in Figure 9. To overcome this issue, only the slower (≤ 10 K/min) cooling rates had to be used [104]. The applicability of this approach for estimating the nucleation activity in a broad range of cooling rates seems generally questionable because of the nonlinearity of $\ln\beta$ vs. ΔT_p^{-2} plots [104,105].

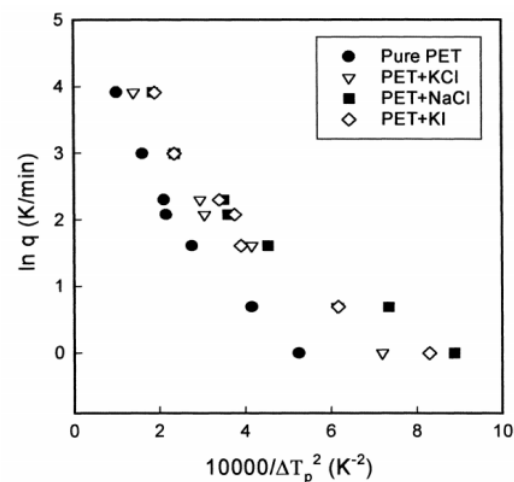


Figure 9. $\ln\beta$ (β is q in Figure) vs. ΔT_p^{-2} plots for PET pure and with different additives crystallized at seven cooling rates (1–50 K/min). Reproduced with permission from Rodriguez–Perez et al. [104]. Copyright 2001 Wiley–VCH.

For large supercoolings (i.e., DSC runs on heating), Dobrova et al. [97,98] proposed a way of estimating the activation energy of viscous flow, whose value, to a good approximation, is equal to E_D in Equation (22) [42]. The original article [97] suggests using the $\ln\beta$ vs. T_p^{-2} plot for this purpose. The later publication [98] changes the suggestion to using the plot of $\ln\beta$ vs. T_p^{-1} , which is similar to the plot used in the Ozawa method [69]. Unexpectedly, some recent studies [106–108] analyze crystallization on heating by means of unusual $\ln\beta$ vs. ΔT_p^{-2} plots. In those plots, ΔT_p is represented as “superheating” with respect to the glass transition temperature T_g , i.e., $\Delta T_p = T_p - T_g$. This is an entirely empirical approach that should not be used for estimating nucleation activity. Recall that the essence of such an estimate is in parameterizing the temperature dependence of crystallization in terms of the nucleation energy barrier, i.e., ΔG^* in Equation (22). The respective temperature dependence is determined by Equation (23), which is derived on thermodynamic grounds and yields ΔT as $T_m - T$, i.e., as the supercooling. The latter controls the magnitude of the nucleation barrier (Equation (23)) in the whole temperature range from T_g to T_m . That is, even for the runs conducted on heating of the glassy samples, one still has to use $\Delta T = T_m - T$ or $\Delta T_p = T_m - T_p$ in order to estimate the nucleation activity. Even then, such an estimate can be problematic simply because the crystallization of glasses occurs at large supercoolings, i.e., under conditions when the contribution of the ΔG^* term can be too small relative to that of the E_D term in Equation (22).

Curiously, the usage of $\Delta T_p = T_p - T_g$ brings to mind a certain analogy with the VTF equation. One of its possible forms is [109]:

$$\ln\beta = Z - \frac{W}{T - T_0} \quad (29)$$

where Z , W , and T_0 are parameters. The VTF equation is commonly used for describing the temperature dependence of viscosity as a more accurate alternative to the Arrhenius equation. In turn, the viscosity of supercooled liquids sets diffusional limitations on the crystallization rate (see Equation (22)). In fact, the exponential Arrhenius E_D term in Equation (22) can be replaced with the respective exponential VTF term, as in the Hoffman–Lauritzen theory discussed in the next section. Then, the activation energy of diffusion becomes temperature-dependent and linked to the VTF parameters as follows [43]:

$$E_D = R \frac{WT^2}{(T - T_0)^2} \quad (30)$$

The reference temperature, T_0 approximately equals $0.75T_g$ [99]. Considering that T_g varies much less with β than T_p , it can be approximated as constant. As a result, one can expect that for DSC on heating the plot of $\ln\beta$ vs. $(T_p - T_g)^{-1}$ (but not vs. $(T_p - T_g)^{-2}$ as mentioned above [108–110]) would yield a reasonable estimate of W (Equation (29)), which can be linked to E_D (Equation (30)).

From the viewpoint of the Arrhenius treatment of crystallization, the most important implication of the Turnbull–Fisher model is that it predicts the Arrhenius activation energy to be temperature-dependent. This dependence can be derived from Equation (22), which describes the temperature dependence of nucleation-driven crystallization. That is, it plays the same role as $k(T)$ in Equation (3). Thus, we can introduce into Equation (3) the temperature dependence appropriate for crystallization by replacing $k(T)$ with the right-hand side of Equation (22). After that, we determine the isoconversional activation energy, E_α , by taking the isoconversional derivative of Equation (3) [110]:

$$E_\alpha = -R \left[\frac{\partial \ln(d\alpha/dt)}{\partial T^{-1}} \right]_\alpha = E_D - \Omega \left[\frac{2T}{(T_m - T)^3} - \frac{1}{(T_m - T)^2} \right] \quad (31)$$

Equation (31) predicts that with increasing temperature, E_α should decrease from E_D to $-\infty$ passing through 0 at the rate maximum. The E_D and $-\infty$ asymptotes are approached at infinitely large and small supercoolings, respectively. Figure 10 depicts an example of such dependence that has been simulated using the E_D and Ω values obtained from fitting the piperine rate data (Figure 7) and the known value of $T_m = 404.7$ K for this compound [111]. The meaning of this dependence is that by parameterizing DSC data on crystallization in terms of the Arrhenius equation, one should obtain from heating runs (large supercoolings) an activation energy that decreases with increasing temperature and/or conversion. Examples of such behavior are seen in Figures 5 and 6. A strong decrease in the activation energy with temperature is also observed in an extensive study of the crystallization of Se [112]. In the case of cooling runs (small supercoolings), one should obtain a negative activation energy that rises with decreasing temperature and/or increasing conversion.

Most importantly, deriving the theoretical temperature dependence for the effective activation energy (Equation (31)) fills the variable and negative E_α values with a clear physical meaning. The meaning of the isoconversional as well as any other effective activation energy, is that it generally is a function of the energy barriers for the individual steps involved in the overall process [84]. In the case of Equation (31), these barriers as E_D and ΔG^* . The latter is estimated by substituting Ω in Equation (23). ΔG^* is temperature-dependent, and an example of such dependence is shown in Figure 10.

In practical terms, the knowledge of the theoretical temperature dependence for the effective activation energy permits developing an original method [113] for analyzing the crystallization kinetics. The method is based on fitting the theoretical dependence to the experimental one. The experimental dependence is best determined from the dependence of E_α on α naturally produced by an isoconversional method. One should be reminded that an isoconversional method suitable for accurately determining the temperature dependence of E_α must be selected from the most accurate methods. In other terms, it should be either

one of the flexible integral methods or the differential method by Friedman, i.e., the method that properly accounts for variability in E_α and is suitable for the data measured on cooling. Once the dependence of E_α on α is determined, it is converted to that of E_α on T by replacing each value of α with the temperature, which is the mean value of all temperatures related to this α at different heating or cooling rates [66,84]. Then, the theoretical E_α vs. T dependence is fitted to the resulting experimental one in order to estimate the parameters E_D and Ω .

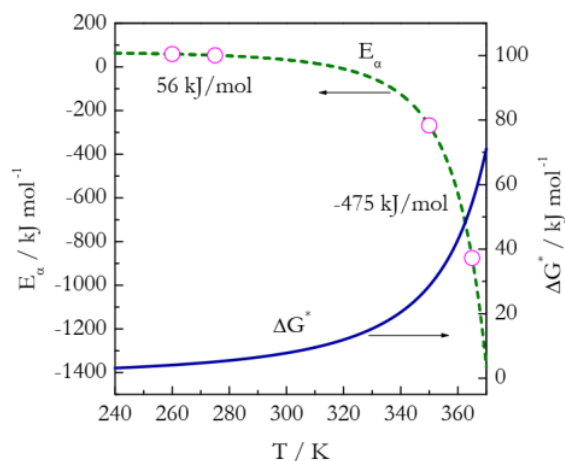


Figure 10. Theoretical temperature dependence of the isoconversional activation energy (dashed line). Circles are the boundaries of the 15 K temperature intervals used for Arrhenius fits in Figure 8. Numerical values by these intervals represent E values at mid-temperatures of the respective intervals. Solid line depicts temperature dependence of the free energy barrier to nucleation.

Of course, one should keep in mind that practically all isoconversional methods are based on the Arrhenius equation, which cannot fit exactly the complex temperature dependence set by Equation (22). In fact, an isoconversional method approximates such dependence with a series of Arrhenius fits corresponding to relatively narrow temperature intervals. For crystallization, the temperature interval related to given α at a series of regular heating or cooling rates typically lies within 10–15 K. Figure 8 provides examples of such fits for two temperature regions of 15 K wide. It is seen that the fit at larger supercoolings is somewhat better than that at the smaller ones. However, both are quite satisfactory, meaning statistically significant based on the correlation coefficients. The actual accuracy of the Arrhenius approximations can be evaluated by comparing the resulting E values (Figure 8) against the E values on the theoretical E vs. T dependence (Figure 10). At the large supercooling, the Arrhenius fit produces $E = 56$ kJ/mol (Figure 8). The theoretical E value determined at the temperature corresponding to the middle of the respective 15 K interval is also $E = 56$ kJ/mol (Figure 10). At the small supercooling, the E value from the Arrhenius fit is -490 kJ/mol (Figure 8), whereas the theoretical one is -475 kJ/mol (Figure 8). While not identical, the values differ only by 3%, which is totally acceptable, especially considering that experimental uncertainties in E commonly reach 5–10%.

The method based on fitting the E_α vs. T dependencies relies on nonlinear optimization. Nevertheless, it possesses a principal advantage over the afore-discussed methods based on linear fits. Recall that those methods work under the simplifying assumption that the crystallization kinetics at large supercoolings can be reduced to the E_D exponential term and at small supercoolings to the ΔG^* exponential term. That is, one exponential term is used in analysis while the other is ignored. The method of nonlinear fitting of E_α vs. T accounts for both exponential terms simultaneously. As a result, the same approach (i.e., the same Equation (22)) is universally applied to the data obtained on heating or cooling as well as to combined (i.e., heating together with cooling) datasets [43,66,83,114].

So far, this method has been applied efficiently to parameterize the kinetics of solid-solid transitions (i.e., crystallization of one crystalline phase from another) [43,66,115] and gelation (i.e., crystallization with the formation of a network or fibrillar structure

that entraps a solvent) [110,114,116]. A recent example is the gelation of several liquids via crystallization of stearic and 12-hydroxystearic acids (12HSA) that was studied in bulk as well as in native (N) and organically modified (OM) 28 nm silica pores [116]. Figure 11 presents kinetic data on the gelation of mineral oil using 12HSA carried out at the cooling rates of 2–16 K/min. The gelation in the nanopores occurs at a markedly lower temperature than in bulk. In other words, the process is more difficult to initiate and, therefore, requires larger supercooling. Isoconversional analysis of the DSC data yields a set of the E_α vs. T dependencies, whose fitting with Equation (31) affords estimating the temperature dependencies of ΔG^* by Equation (23) (Figure 11). The obtained ΔG^* values suggest that the shift of the process in the nanopores to lower temperatures is linked to an increase in the size of the ΔG^* barrier.

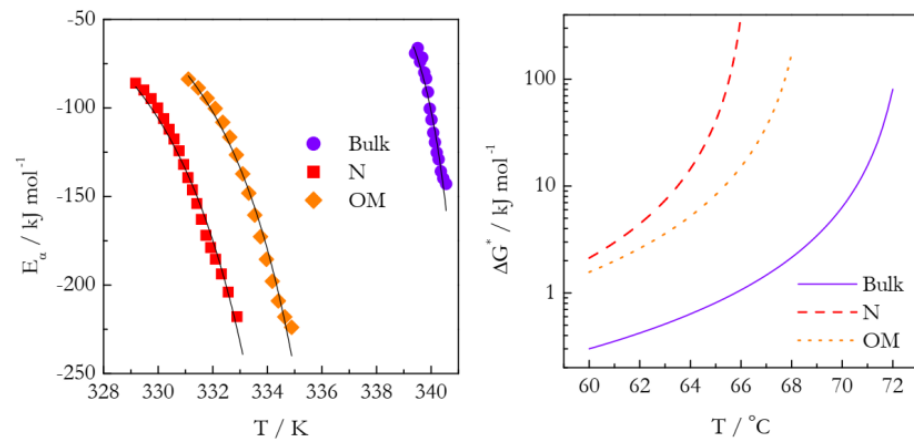


Figure 11. Gelation of mineral oil by crystallization of 12HSA. Left: temperature dependencies of the isoconversional activation energy (points: experimental values; lines: fits to Equation (31)). Right: temperature dependencies of the free energy barrier to nucleation (lines calculated by Equation (23)). Adapted with permission from Espinosa–Dzib and Vyazovkin [116]. Copyright 2021 Elsevier.

In conclusion, it is worth noting that the method based on fitting Equation (22) can be readily expanded to the case when the crystallization rate is determined by the growth of existing nuclei. Since the issue is discussed at length elsewhere [78], only the major points are reiterated here. The rate of growth depends on temperature as [23]:

$$u = u_0 \exp\left(\frac{-E_D}{RT}\right) \left[1 - \exp\left(\frac{\Delta G}{RT}\right)\right] \quad (32)$$

where u_0 is the preexponential factor, and ΔG is the difference in the free energy of the crystalline and liquid phase. ΔG in Equation (32) depends on supercooling via the following relation [25]:

$$\Delta G = \Delta H_m \left(\frac{T - T_m}{T_m}\right) \quad (33)$$

Just as Equation (22), Equation (32) predicts the rate to pass through a maximum. It is again due to the product of the Arrhenian and anti-Arrhenian terms. The latter (bracketed term in Equation (32)) causes the rate to increase with decreasing temperature because ΔG becomes continuously more negative with increasing the supercooling (Equation (33)). Replacing $k(T)$ with the right-hand side of Equation (32) and taking the isoconversional derivative yields the temperature dependence of the isoconversional activation energy:

$$E_\alpha = E_D + \frac{\Delta H_m \exp\left[\frac{\Delta H_m(T - T_m)}{RTT_m}\right]}{\exp\left[\frac{\Delta H_m(T - T_m)}{RTT_m}\right] - 1} \quad (34)$$

The resulting E_α vs. T dependence has an appearance similar to that set by Equation (31) (see Figure 10). That is, E_α has the same E_D and $-\infty$ asymptotes for, respectively, large and small supercoolings and changes its sign at the temperature of the rate maximum. Nevertheless, the E_α vs. T dependencies set by Equations (31) and (34) are not identical and can be differentiated via statistical analysis of the fits to the same dataset [117]. Lastly, the application area of Equation (32) appears to be much more limited than that of Equation (22) because even at large supercoolings, the number of the growth centers still depends strongly on temperature [3], i.e., nucleation remains relevant.

5. Hoffman–Lauritzen Treatment for Broad Temperature Range

Hoffman and Lauritzen [118] modified the Turnbull–Fisher theory to account for the crystallization of long, flexible, and entangled polymer chains that occurs via the chain folding mechanism. According to the Hoffman–Lauritzen theory, the temperature dependence of the microscopically measured growth rate, G , is represented by Equation (35):

$$G = G_0 \exp\left[\frac{-U^*}{R(T - T_\infty)}\right] \exp\left(\frac{-K_g}{T\Delta T f}\right) \quad (35)$$

where G_0 is a pre-exponential factor, U^* is the activation energy of the segmental jump that characterizes molecular diffusion across the interfacial boundary between melt and crystal (its “universal” value is ~ 6.3 kJ/mol), K_g is the energy barrier related to nucleation, $\Delta T = T_m - T$ is the supercooling, T_m is the melting temperature, $f = 2T/(T_m + T)$ is a correction factor, and T_∞ is taken as $T_\infty = T_g - 30$ K, is the temperature at which the viscous flow ceases. In Equation (35),

$$K_g = \frac{2nb\sigma\sigma_e T_m}{\Delta h_f k_B} \quad (36)$$

σ is the lateral surface free energy, σ_e the fold surface free energy (work required to create a new surface), $n = 2$ for the crystallization regime I and III, and 1 for regime II, b is the surface nucleus thickness and Δh_f the enthalpy of melting per unit volume.

In contrast to the Arrhenius equation, Equation (35) takes into account both nucleation and diffusion effects, thus, being able to describe the complex polymers’ crystallization in a broad temperature range. The Hoffman–Lauritzen theory provides an opportunity to determine the values of U^* and K_g that parameterize the effects of both diffusion and nucleation. Vyazovkin and Sbirrazzuoli adapted the Hoffman–Lauritzen theory to nonisothermal DSC data [113,119]. They have shown [113] that the application of the isoconversional derivative to Equation (35) gives rise to Equation (37):

$$E_\alpha = U^* \frac{T^2}{(T - T_\infty)^2} + K_g R \frac{T_m^2 - T^2 - T_m T}{(T_m - T)^2 T} \quad (37)$$

Equation (37) clearly indicates that the resulting isoconversional activation energy is temperature-dependent. The actual dependence is reminiscent of that shown in Figure 10, meaning that for the glass crystallization, E_α is positive and decreases with increasing either T or α , whereas for the melt crystallization, E_α is negative and increases with either increasing α or decreasing T . As discussed in Section 4, an experimental dependence of E_α vs. α is readily convertible to a dependence of E_α vs. T . Then, a nonlinear fit of Equation (37) to the respective experimental dependence of E_α vs. T yields the parameters U^* and K_g .

Predictably, U^* in Equation (35) is not equivalent to E_D in Equation (22). This is because these two equations use different types of temperature dependence for the diffusion term. The dependence is of the Arrhenius type in Equation (22) and of the VTF type in Equation (35). The E_D and U^* values are linked to each other as:

$$E_D = U^* \frac{T^2}{(T - T_\infty)^2} \quad (38)$$

This link is important because the activation energy of diffusion is commonly determined by fitting the temperature dependence of viscosity to the Arrhenius equation, i.e., as E_D . Thus, Equation (38) provides a way of comparing the U^* and E_D barriers. It also follows from Equation (38) that E_D is at least several times larger than U^* .

The method based on fitting Equation (37) has a considerable advantage over the classical approach, which employs laborious isothermal microscopic measurements to determine the growth rate G and is limited to the evaluation of K_g , while U^* is fixed as the “universal” value. Using the latter is hardly a good idea because even in their original work, Hoffman and Lauritzen [120] already found that the best-fit values of U^* vary between 4 and 17 kJ mol⁻¹ and that using a larger constant U^* value leads to estimating a larger value of K_g . Therefore, using both parameters as fit values is a more accurate approach.

In addition, the classical approach is typically limited to microscopic measurements at small supercoolings. In the method based on fitting Equation (37), U^* and K_g are evaluated from much simpler nonisothermal DSC measurements readily conducted in a wide temperature range. In particular, this allows one to fit Equation (37) to a dataset that combines the E_α vs. T dependencies obtained, respectively, from the melt and glass crystallization measurements [83]. The analysis of the combined datasets aids in increasing the precision and accuracy of the U^* and K_g estimates and can help to reveal changes in the crystallization mechanism. Such changes are usually detected as a breakpoint in the E_α vs. T (or vs. α) dependence associated with a significant difference in the K_g values for different regimes of crystallization [121,122].

This method, based on Equation (37), has been repeatedly found to yield U^* and K_g values that are consistent with those determined with the classical microscopic approach [121,122]. Examples of successful applications include crystallization of many polymers such as PET, poly(ethylene oxide), poly(tetrafluoroethylene), poly(dimethylsiloxane), PEF, poly(decylene 2,5-furanoate), poly(butylene succinate), and PEN [60,83,123–131]. It should be stressed that in all the studies where the method is applied, the results are in agreement with the predictions of Equation (37) derived from the Hoffman and Lauritzen theory of crystallization. That is, the general trends are that with increasing temperature, the glass crystallization demonstrates positive decreasing E_α values, and the melt crystallization reveals increasingly negative values of E_α (Figure 12). The latter is a natural manifestation of anti-Arrhenian behavior, i.e., acceleration with decreasing temperature. It arises from the fact that the K_g exponential term in Equation (35) increases with increasing the supercooling. Of course, negative E_α cannot be identified with an energy barrier to a particular step of crystallization. Instead, it is determined (see Equation (37)) by the two barriers U^* and K_g simultaneously and a particular range of T in the close vicinity of T_m . In this temperature range, the crystallization rate is dominated by nucleation. On the other hand, the crystallization rate is dominated by diffusion in a temperature range close to T_g , and Equation (37) predicts positive E_α .

As already mentioned, analysis of the E_α vs. T dependence can provide important insights into the crystallization kinetics and mechanisms. In particular, it can reveal a change in the crystallization mechanism (e.g., the crystallization regime), which is independently verifiable with other techniques. One such example is the nonisothermal crystallization of PEF, which is a fully biobased polyester of a furandicarboxylic acid and a structural analog of PET. It has recently attracted a great deal of attention because of its valuable barrier and mechanical properties. Isoconversional analysis of the melt and glass crystallization expectedly shows negative and positive E_α values that vary with temperature, as predicted by Equation (37) [60]. More importantly, a breakpoint is revealed in the E_α dependence at ~170 °C (Figure 12) that manifests a change in the crystallization regime. This result has been confirmed independently in later studies involving isothermal DSC, Small Angle X-Ray Scattering (SAXS), and Wide-Angle X-ray Scattering (WAXS) measurements [132,133]. More examples of insightful analyses of the E_α dependencies are found elsewhere [121,122].

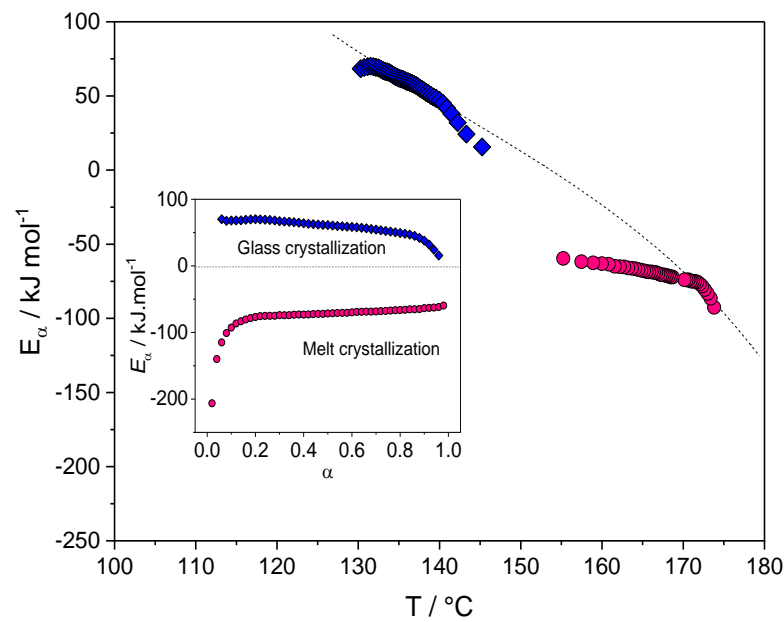


Figure 12. Temperature dependence of E_α for melt (circles) and glass (diamonds) crystallization of PEF. Dashed line is fit of Equation (37) for glass and melt crystallization. Inset shows dependence of E_α on relative degree of crystallinity. Adapted with permission from Codou et al. [60]. Copyright © 2014 Wiley–VCH.

The method based on fitting Equation (37) can be further expanded to perform simulations of the crystallization process. This is accomplished by replacing $k(T)$ in Equation (3) with the temperature dependence that holds for a broad temperature range, i.e., the dependence presented on the right-hand side of the Hoffman–Lauritzen Equation (35). The resulting rate equation is as follows [134]:

$$\frac{d\alpha}{dt} = G(T)f(\alpha) = G_0 \exp\left[\frac{-U^*}{R(T - T_\infty)}\right] \exp\left(\frac{-K_g}{T\Delta T f}\right) f(\alpha) \quad (39)$$

The mathematical function $f(\alpha)$ that describes the crystallization mechanism can be expressed by several equations. It can take the Avrami form:

$$f(\alpha) = m(1 - \alpha)[- \ln(1 - \alpha)]^{1-1/m} \quad (40)$$

It can also take the form of the Sestak–Berggren model [135]: the general form, SB(M, N, P)

$$f(\alpha) = \alpha^M(1 - \alpha)^N[- \ln(1 - \alpha)]^P \quad (41)$$

where M , N , and P are the kinetic exponents, or the truncated one, SB(M, N), as presented in Equation (13).

Parameterizing the experimental crystallization rate in terms of Equation (39) would generally require nonlinear optimization from 4 (Equation (40)) to 6 (Equation (41)) parameters simultaneously, which typically leads to computational problems associated with multiple local minima and mutual correlation of the parameters. Such problems do not appear when optimization is carried out in two steps. First, U^* and K_g are determined by nonlinear fitting of Equation (37). Second, the other parameters are evaluated by nonlinear fitting of Equation (39) while keeping U^* and K_g fixed. This procedure represents a considerable advantage over the simultaneous fitting of all parameters, which is likely to yield incorrect values.

It is noteworthy that evaluating U^* and K_g in the first step of the aforementioned procedure is sufficient to predict an important parameter called the temperature of the maximum of crystal growth rate, T_{max} . As seen from Equation (35), the rate cannot be determined

without knowing G_0 . However, G_0 is a constant in Equation (35), so its value affects the magnitude of the rate but not the position of T_{max} . For this reason, plugging U^* and K_g in the respective exponential terms of Equation (35) and plotting their product as a function of temperature permits predicting the bell-shaped temperature dependence of G/G_0 . Its maximum is T_{max} . The use of this method for the nonisothermal crystallization of PEF has predicted T_{max} around 167 °C when using the parameters obtained for melt crystallization data [60]. This result was confirmed later by isothermal DSC measurements [132–136].

However, simulations of the overall crystallization rate and/or relative extent of crystallinity require employing Equation (39). As already stated, its parameters are effectively determined via the aforementioned two-step optimization procedure. For instance, analysis of the PEF crystallization data demonstrates [134] that the use of the SB model in its either truncated (Equation (13)) or general (Equation (41)) form results in equally accurate simulations. The quality of simulations is illustrated in Figure 13. It is necessary to note that the same set of parameters U^* , K_g , M , and N (Equation (13)) or U^* , K_g , M , N , and P (Equation (41)) is used for both melt and glass data and for all the heating/cooling rates.

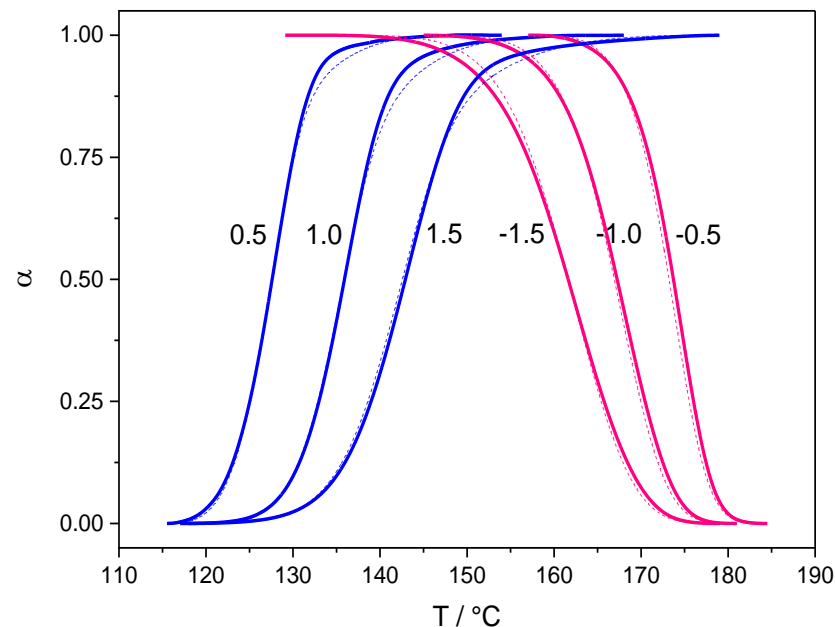


Figure 13. Relative extent of crystallinity (α) vs. temperature (T) for melt and glass crystallization of PEF simulated by combining Equations (13) and (39). Measured and simulated data are shown as solid and dashed lines, respectively. Numbers by the curves are heating (glass crystallization) and cooling (melt crystallization) rate in $\text{K}\cdot\text{min}^{-1}$. Adapted with permission from Guigo et al. [134]. Copyright © 2017 Elsevier B.V.

Although the two-step optimization procedure affords accurate simulations, their accuracy is usually lower for the final stages of crystallization. This is due to the occurrence of processes such as lamellar thickening, secondary crystallization, or others that are not accounted for by Equation (39). It is shown [134] that the accuracy of simulations can be improved by introducing an empirical correction function $h(\alpha)$ as follows:

$$h(\alpha) = \exp[H(\alpha - \alpha_C)] \quad (42)$$

where H is a constant and α_C is a value of the relative extent of crystallinity, above which additional crystallization processes become significant. The $h(\alpha)$ function is introduced into Equation (39) as a multiplier.

An alternative approach to performing simulations is by employing isoconversional predictions. It was originally proposed [137] for the rigid integral methods but later reformulated [43,76] for the flexible ones. Such predictions are also possible with the aid

of the differential method of Friedman [76,138]. Oftentimes, they are termed model-free predictions because they are made without estimating $f(\alpha)$ or $g(\alpha)$. In the case of the flexible integral methods, the only estimation needed is the E_α -dependence. Figure 14 provides an example of isoconversional simulations for the glass and melt crystallization of PEF [134]. Remarkably, the simulations appear even more accurate than the model-based ones shown in Figure 13. The caveat, though, is that the glass and melt crystallization simulations have to be performed using the corresponding E_α -dependencies.

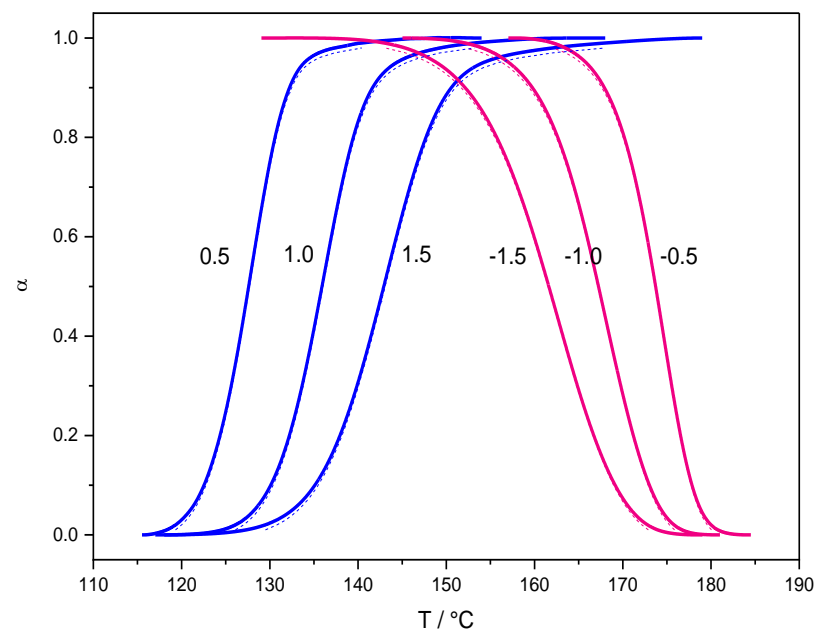


Figure 14. Relative extent of crystallinity (α) vs. temperature (T) for melt and glass crystallization of PEF simulated as isoconversional (model-free) predictions. Measured and simulated data are shown as solid and dashed lines, respectively. Numbers by the curves are heating (glass crystallization) and cooling (melt crystallization) rate in $\text{K}\cdot\text{min}^{-1}$. Adapted with permission from Guigo et al. [134]. Copyright © 2017 Elsevier B.V.

It must be emphasized that the afore-discussed approaches to simulation are equally valid when the crystallization kinetics is parameterized in terms of the Turnbull–Fisher model (Section 4). That is, the E_D and Ω parameters determined by Equation (31) can be used for estimating the value of T_{max} . Moreover, the crystallization rate can be simulated with an equation similar to Equation (39) with the temperature dependence, $G(T)$, having the Turnbull–Fisher form from Equation (22). The method of isoconversional predictions is applicable as well.

In conclusion, it should be added that the method of nonparametric kinetics (NPK) [139] can separate the crystallization rate into the temperature and conversion dependencies without making any assumptions about their mathematical forms. The temperature dependence can then be fitted using the Hoffman–Lauritzen equation, and the conversion dependence using the Avrami or SB equation. The capabilities of the NPK method have been illustrated for the melt crystallization of isotactic polypropylene [140]. It should also be borne in mind that Equation (39) can be cast in the isoconversional form so that U^* and K_g are estimated from DSC data as a function of α [141,142]. Potentially, such dependencies may offer additional insights into the complexities of the crystallization kinetics. The approach is exemplified by the crystallization of PET and polyamide 6 [141] as well as of PEF [142].

6. Conclusions

DSC is the most common technique for measuring the overall crystallization rate. The measurements are primarily conducted under nonisothermal conditions that allow one to explore a broad temperature range. Analysis of the nonisothermal crystallization kinetics is dominated by approaches based on the Avrami and Arrhenius equations. The application of the Avrami model to nonisothermal data is subject to very restrictive assumptions. Contrary to popular belief, this model is not universally applicable to every crystallization, and its applicability must necessarily be tested. The general autocatalytic (a.k.a. truncated SB) model provides a more universal alternative. In turn, the Arrhenius equation is only an approximation to the actual bell-shaped temperature dependence of the crystallization rate and, thus, should only be applied to a narrow temperature range, probably not broader than 20 K. Whatever the temperature range, the applicability of the Arrhenius approximation is readily tested as invariability of the isoconversional activation energy. Proper isoconversional methods (i.e., differential or flexible integral ones) accurately approximate the temperature dependence of the crystallization rate by a series of the Arrhenius equations, each of which corresponds to its own narrow temperature interval. Thanks to this feature, the methods are applicable to the whole temperature range from T_g to T_m or, in other words, suitable for kinetic analysis of both glass and melt crystallization. In such a broad temperature range, the isoconversional activation energy is unavoidably variable. Its temperature dependence can be parameterized in terms of the Turnbull–Fisher or Hoffman–Lauritzen theories, and the resulting parameters can then be meaningfully interpreted and used for kinetic simulations. This modern-day approach has a significant advantage over the earlier methods that offer very unsophisticated kinetic treatment, which is specific to either glass or melt crystallization only.

Author Contributions: Conceptualization, S.V.; writing—original draft preparation, S.V. and N.S.; writing—review and editing, S.V. and N.S. All authors have read and agreed to the published version of the manuscript.

Funding: This research received no external funding.

Data Availability Statement: Not applicable.

Conflicts of Interest: The authors declare no conflict of interest.

References

1. Available online: <https://scopus.com> (accessed on 30 March 2023).
2. Henderson, D.W. Thermal analysis of non-isothermal crystallization kinetic in glass forming liquids. *J. Non-Cryst. Solids* **1979**, *30*, 301–315. [[CrossRef](#)]
3. Yinnon, H.; Uhlmann, D.R. Applications of thermoanalytical techniques to the study of crystallization kinetics in glass-forming liquids, Part I: Theory. *J. Non-Cryst. Solids* **1983**, *54*, 253–275. [[CrossRef](#)]
4. Di Lorenzo, M.L.; Silvestre, C. Non-isothermal crystallization of polymers. *Prog. Polym. Sci.* **1999**, *24*, 917–950. [[CrossRef](#)]
5. Vyazovkin, S.; Burnham, A.K.; Criado, J.M.; Pérez-Maqueda, L.A.; Popescu, C.; Sbirrazzuoli, N. ICTAC Kinetics Committee recommendations for performing kinetic computations on thermal analysis data. *Thermochim. Acta* **2011**, *520*, 1–19. [[CrossRef](#)]
6. Vyazovkin, S.; Burnham, A.K.; Favregeon, L.; Koga, N.; Moukhina, E.; Pérez-Maqueda, L.A.; Sbirrazzuoli, N. ICTAC Kinetics Committee recommendations for analysis of multi-step kinetics. *Thermochim. Acta* **2020**, *689*, 178597. [[CrossRef](#)]
7. Borchardt, H.J.; Daniels, F. The application of differential thermal analysis to the study of reaction kinetics. *J. Am. Chem. Soc.* **1957**, *79*, 41–46. [[CrossRef](#)]
8. Sestak, J. Ignoring heat inertia impairs accuracy of determination of activation energy in thermal analysis. *Int. J. Chem. Kinet.* **2019**, *51*, 74–80. [[CrossRef](#)]
9. Vyazovkin, S. How much is the accuracy of activation energy affected by ignoring thermal inertia? *Int. J. Chem. Kinet.* **2020**, *52*, 23–28. [[CrossRef](#)]
10. Matusita, K.; Sakka, S.; Matsui, Y. Determination of the activation energy for crystal growth by differential thermal analysis. *J. Mater. Sci.* **1975**, *10*, 961–966. [[CrossRef](#)]
11. Hohne, G.W.H.; Hemminger, W.F.; Flammersheim, H.J. *Differential Scanning Calorimetry*, 2nd ed.; Springer: Berlin, Germany, 2003.
12. Perez, A.; Lopez-Olmedo, J.P.; Farjas, J.; Roura, P. Isoconversional analysis of copper recrystallization. *J. Therm. Anal. Calorim.* **2016**, *125*, 667–672. [[CrossRef](#)]

13. Kossoy, A. Effect of thermal inertia-induced distortions of DSC data on the correctness of the kinetics evaluated. *J. Therm. Anal. Calorim.* **2021**, *143*, 599–608. [[CrossRef](#)]
14. Koci, V.; Sestak, J.; Cerny, R. Thermal inertia and evaluation of reaction kinetics: A critical review. *Measurement* **2022**, *198*, 111354. [[CrossRef](#)]
15. Vyazovkin, S.; Chrissafis, K.; Di Lorenzo, M.L.; Koga, N.; Pijolat, M.; Roduit, B.; Sbirrazzuoli, N.; Suñol, J.J. ICTAC Kinetics Committee recommendations for collecting experimental thermal analysis data for kinetic computations. *Thermochim. Acta* **2014**, *590*, 1–23. [[CrossRef](#)]
16. Lyon, R.E.; Safronava, N.; Senese, J.; Stoliarov, S.I. Thermokinetic model of sample response in nonisothermal analysis. *Thermochim. Acta* **2012**, *545*, 82–89. [[CrossRef](#)]
17. ASTM E537-12; Standard Test Method for The Thermal Stability of Chemicals by Differential Scanning Calorimetry. ASTM International: West Conshohocken, PA, USA, 2013.
18. Burnham, A.K.; Stanford, V.L.; Vyazovkin, S.; Kahl, E.M. Effect of pressure on TATB and LX-17 thermal decomposition. *Thermochim. Acta* **2021**, *699*, 178908. [[CrossRef](#)]
19. Johnson, W.A.; Mehl, K.F. Reaction kinetics in processes of nucleation and growth. *Trans. Am. Inst. Min. Metall. Eng.* **1939**, *135*, 416–458.
20. Avrami, M. Kinetics of phase change. I. General theory. *J. Chem. Phys.* **1939**, *7*, 1103–1112. [[CrossRef](#)]
21. Erofeev, B.V. A generalized equation of chemical kinetics and its application in reaction involving solids. *CR Acad. Sci. URSS* **1946**, *52*, 511–514.
22. Kolmogorov, N.N. On the statistical theory of the crystallization of metals. *Bull. Acad. Sci. USSR Math. Ser.* **1937**, *1*, 355–359.
23. Christian, J.W. *The Theory of Transformations in Metals and Alloys*; Pergamon: Amsterdam, The Netherlands, 2002.
24. Schultz, J.M. *Polymer Crystallization*; ACS & Oxford University Press: New York, NY, USA, 2001.
25. Mandelkern, L. *Crystallization of Polymers*; Cambridge University Press: Cambridge, UK, 2004; Volume 2.
26. Blázquez, J.S.; Romero, F.J.; Conde, C.F.; Conde, A. A Review of Different Models Derived from Classical Kolmogorov, Johnson and Mehl, and Avrami (KJMA) Theory to Recover Physical Meaning in Solid-State Transformations. *Phys. Status Solidi B* **2022**, *259*, 2100524. [[CrossRef](#)]
27. Morgan, L.B. Crystallization phenomena in polymers II. The course of crystallization. *Philos. Trans. R. Soc. A* **1954**, *247*, 13–22.
28. Flynn, J.H. The ‘Temperature Integral’—Its use and abuse. *Thermochim. Acta* **1997**, *300*, 83–92. [[CrossRef](#)]
29. Matusita, K.; Komatsu, T.; Yokota, R. Kinetics of non-isothermal crystallization process and activation energy for crystal growth in amorphous materials. *J. Mater. Sci.* **1984**, *19*, 291–296. [[CrossRef](#)]
30. Malek, J. The applicability of Johnson-Mehl-Avrami model in the thermal analysis of the crystallization kinetics of glasses. *Thermochim. Acta* **1995**, *267*, 61–73. [[CrossRef](#)]
31. Lopez-Alemay, P.L.; Vazquez, J.; Villares, P.; Jimenez-Garay, R. Kinetic study on non-isothermal crystallization in glassy materials: Application to the $\text{Sb}_{0.12}\text{As}_{0.40}\text{Se}_{0.48}$ alloy. *J. Alloys Compd.* **1999**, *285*, 185–193. [[CrossRef](#)]
32. Farjas, J.; Roura, P. Modification of the Kolmogorov–Johnson–Mehl–Avrami rate equation for non-isothermal experiments and its analytical solution. *Acta Mater.* **2006**, *54*, 5573–5579. [[CrossRef](#)]
33. Vyazovkin, S. Jeziorny Method Should Be Avoided in Avrami Analysis of Nonisothermal Crystallization. *Polymers* **2023**, *15*, 197. [[CrossRef](#)]
34. Malek, J.; Watanabe, A.; Mitsuhashi, T. Crystallization kinetics of amorphous RuO_2 . *Thermochim. Acta* **1996**, *282–283*, 131–142. [[CrossRef](#)]
35. Sunol, J.J.; Clavaguera, N.; Mora, M.T. Thermal stability study of Fe-Ni-based alloys. *J. Therm. Anal.* **1998**, *52*, 853–862. [[CrossRef](#)]
36. Sunol, J.J.; Berlanga, R.; Clavaguera-Mora, M.T.; Clavaguera, N. Modeling crystallization processes: Transformation diagrams. *Acta Mater.* **2002**, *50*, 4783–4790. [[CrossRef](#)]
37. Sunol, J.J. Transformation diagrams: Isoconversional method from calorimetric data. *J. Therm. Anal. Calorim.* **2003**, *72*, 25–33. [[CrossRef](#)]
38. Kelly, C.A.; Hay, J.N.; Turner, R.P.; Jenkins, M.J. The Effect of a Secondary Process on the Analysis of Isothermal Crystallisation Kinetics by Differential Scanning Calorimetry. *Polymers* **2020**, *12*, 19. [[CrossRef](#)] [[PubMed](#)]
39. de Bruijn, T.J.W.; de Jong, W.A.; van den Berg, P.J. Kinetic parameters in Avrami-Erofeev type reactions from isothermal and non-isothermal experiments. *Thermochim. Acta* **1981**, *45*, 315–325. [[CrossRef](#)]
40. Avrami, M. Kinetics of Phase Change. II Transformation Time Relations for Random Distribution of Nuclei. *J. Chem. Phys.* **1940**, *8*, 212–224. [[CrossRef](#)]
41. Henderson, D.W. Experimental analysis of nonisothermal transformations involving nucleation and growth. *J. Therm. Anal.* **1979**, *15*, 325–331. [[CrossRef](#)]
42. Vyazovkin, S. Activation energies and temperature dependencies of the rates of crystallization and melting of polymers. *Polymers* **2020**, *12*, 1070. [[CrossRef](#)]
43. Vyazovkin, S. *Isoconversional Kinetics of Thermally Stimulated Processes*; Springer: Heidelberg, Germany, 2015.
44. Hong, P.D.; Chung, W.T.; Hsu, C.F. Crystallization kinetics and morphology of poly(trimethylene terephthalate). *Polymer* **2002**, *43*, 3335–3343. [[CrossRef](#)]
45. Hancock, J.D.; Sharp, J.H. Method of Comparing Solid-state Kinetic Data and Its Application to the Decomposition of Kaolinite, Brucite, and BaCO_3 . *J. Am. Ceram. Soc.* **1972**, *55*, 74–77. [[CrossRef](#)]

46. Malek, J. Kinetic analysis of crystallization processes in amorphous materials. *Thermochim. Acta* **2000**, *355*, 239–253. [[CrossRef](#)]
47. Svoboda, R. Crystallization of glasses—When to use the Johnson-Mehl-Avrami kinetics? *J. Eur. Ceram. Soc.* **2021**, *41*, 7862–7867. [[CrossRef](#)]
48. Malek, J. Crystallization kinetics by thermal analysis. *J. Therm. Anal. Calorim.* **1999**, *56*, 763–769. [[CrossRef](#)]
49. Perez-Maqueda, L.A.; Criado, J.M.; Sanchez-Jimenez, P.E. Combined Kinetic Analysis of Solid-State Reactions: A Powerful Tool for the Simultaneous Determination of Kinetic Parameters and the Kinetic Model without Previous Assumptions on the Reaction Mechanism. *J. Phys. Chem. A* **2006**, *110*, 12456–12462. [[CrossRef](#)] [[PubMed](#)]
50. Svoboda, R.; Brandova, D.; Malek, J. Non-isothermal crystallization kinetics of GeTe₄ infrared glass. *J. Therm. Anal. Calorim.* **2016**, *123*, 195–204. [[CrossRef](#)]
51. Svoboda, R.; Brandova, D. Crystal growth from mechanically induced defects. A phenomenon observed for glassy materials. *J. Therm. Anal. Calorim.* **2017**, *127*, 799–808. [[CrossRef](#)]
52. Ekawa, B.; Stanford, V.; Vyazovkin, S. Isoconversional kinetics of vaporization of nanoconfined liquids. *J. Mol. Liq.* **2021**, *327*, 114824. [[CrossRef](#)]
53. Galukhin, A.; Nikolaev, I.; Nosov, R.; Vyazovkin, S. Solid-state polymerization of a novel cyanate ester based on 4-*tert*-butylcalix[6]arene. *Polym. Chem.* **2020**, *11*, 4115–4123. [[CrossRef](#)]
54. Brown, M.E.; Dollimore, D.; Galwey, A.K. *Reactions in the Solid State, Comprehensive Chemical Kinetics*; Elsevier: Amsterdam, The Netherlands, 1980; Volume 22.
55. Perez-Maqueda, L.A.; Criado, J.M.; Malek, J. Combined kinetic analysis for crystallization kinetics of non-crystalline solids. *J. Non-Cryst. Solids* **2003**, *320*, 84–91. [[CrossRef](#)]
56. Vyazovkin, S.; Wight, C.A. Model-Free and Model-Fitting Approaches to Kinetic Analysis of Isothermal and Nonisothermal Data. *Thermochim. Acta* **1999**, *340–341*, 53–68. [[CrossRef](#)]
57. Vyazovkin, S. Comments on multiple publications reporting single heating rate kinetics. *Appl. Organomet. Chem.* **2023**, *37*, e6929. [[CrossRef](#)]
58. Muravyev, N.V.; Vyazovkin, S. The status of pyrolysis kinetics studies by thermal analysis: Quality is not as good as it should and can readily be. *Thermo* **2022**, *2*, 435–452. [[CrossRef](#)]
59. Ozawa, T. Kinetics of nonisothermal crystallization. *Polymer* **1971**, *12*, 150–158. [[CrossRef](#)]
60. Codou, A.; Guigo, N.; van Berkel, J.; de Jong, E.; Sbirrazzuoli, N. Nonisothermal Crystallization Kinetics of biobased Poly(ethylene 2,5-furandicarboxylate) synthesized via direct esterification process. *Macromol. Chem. Phys.* **2014**, *215*, 2065–2074. [[CrossRef](#)]
61. Toda, A. A reinterpretation of the Ozawa model for non-isothermal crystallization at fixed scan rates. *Thermochim. Acta* **2022**, *707*, 179086. [[CrossRef](#)]
62. Toda, A. A note on the kinetics of non-isothermal crystallization of polymers. *Thermochim. Acta* **2022**, *713*, 179244. [[CrossRef](#)]
63. Jeziorny, A. Parameters characterizing the kinetics of the non-isothermal crystallization of poly(ethylene terephthalate) determined by d.s.c. *Polymer* **1978**, *19*, 1142–1144. [[CrossRef](#)]
64. Zhang, Z.; Xiao, C.; Dong, Z. Comparison of the Ozawa and modified Avrami models of polymer crystallization under nonisothermal conditions using a computer simulation method. *Thermochim. Acta* **2007**, *466*, 22–28. [[CrossRef](#)]
65. Kourtidou, D.; Chrissafis, K. Nonisothermal Crystallization Kinetics: Studying the Validity of Different Johnson–Mehl–Avrami–Erofeev–Kolmogorov (JMAEK) Based Equations. *Thermochim. Acta* **2021**, *704*, 179030.
66. Vyazovkin, S. Modern isoconversional kinetics: From Misconceptions to Advances. In *The Handbook of Thermal Analysis & Calorimetry, Volume 6: Recent Advances, Techniques and Applications*, 2nd ed.; Vyazovkin, S., Koga, N., Schick, C., Eds.; Elsevier: Amsterdam, The Netherlands, 2018; pp. 131–172.
67. Friedman, H.L. Kinetics of thermal degradation of char-forming plastics from thermogravimetry. Application to a phenolic plastic. *J. Polym. Sci. Part C* **1964**, *6*, 183–195. [[CrossRef](#)]
68. Abu El-Oyoun, M. DSC studies on the transformation kinetics of two separated crystallization peaks of Si_{12.5}Te_{87.5} chalcogenide glass: An application of the theoretical method developed and isoconversional method. *Mater. Chem. Phys.* **2011**, *131*, 495–506. [[CrossRef](#)]
69. Ozawa, T. A new method of analyzing thermogravimetric data. *Bull. Chem. Soc. Jpn.* **1965**, *38*, 1881–1886. [[CrossRef](#)]
70. Flynn, J.H.; Wall, L.A. A quick, direct method for the determination of activation energy from thermogravimetric data. *J. Polym. Sci. C Polym. Lett.* **1966**, *4*, 323–328. [[CrossRef](#)]
71. Flynn, J.H.; Wall, L.A. General treatment of the thermogravimetry of polymers. *J. Res. Nat. Bur. Stand. Part A* **1966**, *70*, 487–523. [[CrossRef](#)] [[PubMed](#)]
72. Akahira, T.; Sunose, T. Method of determining activation deterioration constant of electrical insulating materials. *Res. Rep. Chiba Inst. Technol. (Sci. Technol.)* **1971**, *16*, 22–31.
73. Starink, M.J. The determination of activation energy from linear heating rate experiments: A comparison of the accuracy of isoconversion methods. *Thermochim. Acta* **2003**, *404*, 163–176. [[CrossRef](#)]
74. Vyazovkin, S. Modification of the integral isoconversional method to account for variation in the activation energy. *J. Comput. Chem.* **2001**, *22*, 178–183. [[CrossRef](#)]
75. Ortega, A. A simple and precise linear integral method for isoconversional data. *Thermochim. Acta* **2008**, *474*, 81–86. [[CrossRef](#)]
76. Vyazovkin, S.; Achilias, D.; Fernandez-Francos, X.; Galukhin, A.; Sbirrazzuoli, N. ICTAC Kinetics Committee recommendations for analysis of thermal polymerization kinetics. *Thermochim. Acta* **2022**, *714*, 179243. [[CrossRef](#)]

77. Kissinger, H.E. Reaction kinetics in differential thermal analysis. *Anal. Chem.* **1957**, *29*, 1702–1706. [[CrossRef](#)]
78. Vyazovkin, S. Kissinger Method in Kinetics of Materials: Things to Beware and Be Aware of. *Molecules* **2020**, *25*, 2813. [[CrossRef](#)]
79. Vyazovkin, S. Is the Kissinger Equation Applicable to the Processes that Occur on Cooling? *Macromol. Rapid Commun.* **2002**, *23*, 771–775. [[CrossRef](#)]
80. Zhang, Z.; Chen, J.; Liu, H.; Xiao, C. Applicability of Kissinger model in nonisothermal crystallization assessed using a computer simulation method. *J. Therm. Anal. Calorim.* **2014**, *117*, 783–787. [[CrossRef](#)]
81. Shi, C.-B.; Wang, H.; Seo, M.-D.; Cho, J.-W.; Kim, S.-H. Evaluation of Matusita Equation and Its Modified Expression for Determining Activation Energy Associated with Melt Crystallization. *Metall. Mater. Trans. B* **2014**, *45*, 1987–1991. [[CrossRef](#)]
82. Matusita, K.; Sakka, S. Kinetic study on crystallization of glass by differential thermal analysis—Criterion on application of Kissinger plot. *J. Non-Cryst. Solids* **1980**, *38–39*, 741–746. [[CrossRef](#)]
83. Vyazovkin, S.; Dranca, I. Isoconversional Analysis of Combined Melt and Glass Crystallization Data. *Macromol. Chem. Phys.* **2006**, *207*, 20–25. [[CrossRef](#)]
84. Vyazovkin, S. A time to search: Finding the meaning of variable activation energy. *Phys. Chem. Chem. Phys.* **2016**, *18*, 18643–18656. [[CrossRef](#)]
85. Svoboda, R.; Malek, J. Applicability of Fraser–Suzuki function in kinetic analysis of complex crystallization processes. *J. Therm. Anal. Calorim.* **2013**, *111*, 1045–1056. [[CrossRef](#)]
86. Brandova, D.; Svoboda, R.; Olmrova Zmrhalova, Z.; Chovanec, J.; Bulanek, R.; Romanova, J. Crystallization kinetics of glassy materials: The ultimate kinetic complexity? *J. Therm. Anal. Calorim.* **2018**, *134*, 825–834. [[CrossRef](#)]
87. Liland, K.H.; Svoboda, R.; Luciano, G.; Muravyev, N. Neural networks applied in kinetic analysis of complex nucleation-growth processes: Outstanding solution for fully overlapping reaction mechanisms. *J. Non-Cryst. Solids* **2022**, *588*, 121640. [[CrossRef](#)]
88. Sbirrazzuoli, N.; Brunel, D.; Elegant, L. Neural networks for kinetic parameters determination, signal filtering and deconvolution in thermal analysis. *J. Therm. Anal.* **1997**, *49*, 1553–1564. [[CrossRef](#)]
89. Sbirrazzuoli, N.; Brunel, D. Computational neural networks for mapping calorimetric data: Application of feed-forward neural networks to kinetic parameters determination and signals filtering. *Neural. Comput. Appl.* **1997**, *5*, 20–32. [[CrossRef](#)]
90. Tammann, G. Ueber die Abhängigkeit der Zahl der Kerne, welche sich in verschiedenen unterkühlten Flüssigkeiten bilden, von der Temperatur. *Z. Phys. Chem.* **1898**, *25*, 441–479. [[CrossRef](#)]
91. Turnbull, D.; Fisher, J.C. Rate of nucleation in condensed systems. *J. Chem. Phys.* **1949**, *17*, 71–73. [[CrossRef](#)]
92. Liavitskaya, T.; Vyazovkin, S. Discovering the kinetics of thermal decomposition during continuous cooling. *Phys. Chem. Chem. Phys.* **2016**, *18*, 32021–32030. [[CrossRef](#)] [[PubMed](#)]
93. Liavitskaya, T.; Vyazovkin, S. Kinetics of thermal polymerization can be studied during continuous cooling. *Macromol. Rapid Commun.* **2018**, *39*, 1700624. [[CrossRef](#)] [[PubMed](#)]
94. Clavaguera, N.; Saurina, J.; Lheritier, J.; Masse, J.; Chauvet, A.; Clavaguera-Mora, M.T. Eutectic mixtures for pharmaceutical applications: A thermodynamic and kinetic study. *Thermochim. Acta* **1997**, *290*, 173–180. [[CrossRef](#)]
95. Sunol, J.J. Modeling Polymer Crystallization: T-CR-T Diagram Construction. *Int. J. Polym. Mater. Polym. Biomater.* **2002**, *51*, 49–56. [[CrossRef](#)]
96. Berlanga, R.; Sunol, J.J.; Saurina, J. Polymer Crystallization: A DSC Approach to Building the T-CR-T Diagram. *Macromol. Theory Simul.* **2008**, *17*, 103–108. [[CrossRef](#)]
97. Dobрева, A.; Stoyanov, A.; Gutzow, I. Analysis of differential scanning calorimetry data on the nonisothermal kinetics of crystallization in polymer melts. *J. Appl. Polym. Sci. (Appl. Polym. Symp.)* **1991**, *48*, 473–480. [[CrossRef](#)]
98. Dobрева, A.; Gutzow, I. Activity of substrates in the catalyzed nucleation of glass-forming melts. II. Experimental evidence. *J. Non-Cryst. Solids* **1993**, *162*, 13–25. [[CrossRef](#)]
99. Gutzow, I.S.; Schmelzer, J.W.P. *The Vitreous State. Thermodynamics, Structure, Rheology, and Crystallization*, 2nd ed.; Springer: Heidelberg, Germany, 2013.
100. Barandiaran, J.M.; Colmenero, J. Continuous cooling approximation for the formation of a glass. *J. Non-Cryst. Solids* **1981**, *46*, 277–287. [[CrossRef](#)]
101. Cabral, A.A.; Cardoso, A.A.D.; Zanutto, E.D. Glass-forming ability versus stability of silicate glasses. I. Experimental test. *J. Non-Cryst. Solids* **2003**, *320*, 1–8. [[CrossRef](#)]
102. Ray, C.S.; Reis, S.T.; Brow, R.K.; Holand, W.; Rheinberger, V. A new DTA method for measuring critical cooling rate for glass formation. *J. Non-Cryst. Solids* **2005**, *351*, 1350–1358. [[CrossRef](#)]
103. Baird, J.A.; van Eerdenbrugh, B.; Taylor, L.S. A Classification System to Assess the Crystallization Tendency of Organic Molecules from Undercooled Melts. *J. Pharm. Sci.* **2010**, *99*, 3787–3806. [[CrossRef](#)] [[PubMed](#)]
104. Rodriguez-Perez, M.A.; Vasiliev, T.; Dobрева-Velleva, A.; de Saja, J.A.; Gutzow, I.; Velasco, J.I. The activity of inorganic substrates in the catalyzed nucleation of different polymer melts. *Macromol. Symp.* **2001**, *169*, 137–142. [[CrossRef](#)]
105. Schawe, J.E.K.; Potschke, P.; Alig, I. Nucleation efficiency of fillers in polymer crystallization studied by fast scanning calorimetry: Carbon nanotubes in polypropylene. *Polymer* **2017**, *116*, 160–172. [[CrossRef](#)]
106. Papageorgiou, G.Z.; Achilias, D.S.; Nanaki, S.; Beslikas, T.; Bikiaris, D. PLA nanocomposites: Effect of filler type on non-isothermal crystallization. *Thermochim. Acta* **2010**, *511*, 129–139. [[CrossRef](#)]

107. Bussiere, P.O.; Therias, S.; Gardette, J.-L.; Murariu, M.; Dubois, P.; Baba, M. Effect of ZnO nanofillers treated with triethoxy caprylylsilane on the isothermal and non-isothermal crystallization of poly(lactic acid). *Phys. Chem. Chem. Phys.* **2012**, *14*, 12301–12308. [[CrossRef](#)]
108. Li, Y.; Han, C.; Yu, Y.; Xiao, L.; Shao, Y. Isothermal and nonisothermal cold crystallization kinetics of poly(L-lactide)/functionalized eggshell powder composites. *J. Therm. Anal. Calorim.* **2018**, *131*, 2213–2223. [[CrossRef](#)]
109. Schawe, J.E.K. Vitrification in a wide cooling rate range: The relations between cooling rate, relaxation time, transition width, and fragility. *J. Chem. Phys.* **2014**, *141*, 184905. [[CrossRef](#)]
110. Chen, K.; Baker, A.N.; Vyazovkin, S. Concentration Effect on Temperature Dependence of Gelation Rate in Aqueous Solutions of Methylcellulose. *Macromol. Chem. Phys.* **2009**, *210*, 211–216. [[CrossRef](#)]
111. Lide, D.R. (Ed.) *CRC Handbook of Chemistry and Physics*, 83rd ed.; CRC Press: Boca Raton, FL, USA, 2002.
112. Malek, J.; Svoboda, R. Kinetic Processes in Amorphous Materials Revealed by Thermal Analysis: Application to Glassy Selenium. *Molecules* **2019**, *24*, 2725. [[CrossRef](#)] [[PubMed](#)]
113. Vyazovkin, S.; Sbirrazzuoli, N. Isoconversional approach to evaluating the Hoffman-Lauritzen parameters (U^* and K_g) from the overall rates of nonisothermal crystallization. *Macromol. Rapid Commun.* **2004**, *25*, 733–738. [[CrossRef](#)]
114. Guigo, N.; Sbirrazzuoli, N.; Vyazovkin, S. Atypical gelation in gelatin solutions probed by ultrafast calorimetry. *Soft Matter* **2012**, *8*, 7116–7121. [[CrossRef](#)]
115. Farasat, R.; Yancey, B.; Vyazovkin, S. High Temperature Solid-solid Transition in Ammonium Chloride Confined to Nanopores. *J. Phys. Chem. C* **2013**, *117*, 13713–13721. [[CrossRef](#)]
116. Espinosa-Dzib, A.; Vyazovkin, S. Nanoconfined gelation in systems based on stearic and 12-hydroxystearic acids: A calorimetric study. *J. Mol. Liq.* **2021**, *335*, 116191. [[CrossRef](#)]
117. Liavitskaya, T.; Birx, L.; Vyazovkin, S. Melting Kinetics of Superheated Crystals of Glucose and Fructose. *Phys. Chem. Chem. Phys.* **2017**, *19*, 26056–26064. [[CrossRef](#)]
118. Hoffman, J.D.; Davis, G.T.; Lauritzen, J.I. *Treatise on Solid State Chemistry*; Hannay, N., Ed.; Plenum: New York, NY, USA, 1976; Volume 3, p. 497.
119. Vyazovkin, S.; Sbirrazzuoli, N. Isoconversional analysis of the nonisothermal crystallization of a polymer melt. *Macromol. Rapid Commun.* **2002**, *23*, 766–770. [[CrossRef](#)]
120. Hoffman, J.D.; Lauritzen, J.I. Crystallization of bulk polymers with chain folding: Theory of growth of lamellar spherulites. *J. Res. Natl. Bur. Stand.* **1961**, *65A*, 297–336. [[CrossRef](#)]
121. Vyazovkin, S.; Sbirrazzuoli, N. Isoconversional Kinetic Analysis of Thermally Stimulated Processes in Polymers. *Macromol. Rapid Commun.* **2006**, *27*, 1515–1532. [[CrossRef](#)]
122. Vyazovkin, S. Isoconversional kinetics of polymers: The decade past. *Macromol. Rapid Commun.* **2017**, *38*, 1600615. [[CrossRef](#)]
123. Vyazovkin, S.; Sbirrazzuoli, N. Estimating the activation energy for nonisothermal crystallization of polymer melts. *J. Therm. Anal. Calorim.* **2003**, *72*, 681–686. [[CrossRef](#)]
124. Vyazovkin, S.; Stone, J.; Sbirrazzuoli, N. Hoffman-Lauritzen parameters for nonisothermal crystallization of poly(ethylene terephthalate) and poly(ethylene oxide) melts. *J. Therm. Anal. Calorim.* **2005**, *80*, 177–180. [[CrossRef](#)]
125. Bosq, N.; Guigo, N.; Zhuravlev, E.; Sbirrazzuoli, N. Non-isothermal crystallization of polytetrafluoroethylene in wide range of cooling rates. *J. Phys. Chem. B* **2013**, *117*, 3407–3415. [[CrossRef](#)] [[PubMed](#)]
126. Bosq, N.; Guigo, N.; Persello, J.; Sbirrazzuoli, N. Melt and glass crystallization of PDMS and PDMS silica nanocomposites. *Phys. Chem. Chem. Phys.* **2014**, *16*, 7830–7840. [[CrossRef](#)] [[PubMed](#)]
127. Tsanaktsis, V.; Bikiaris, D.N.; Guigo, N.; Exarhopoulos, S.; Papageorgiou, D.G.; Sbirrazzuoli, N.; Papageorgiou, G.Z. Synthesis, properties and thermal behavior of Poly(decylene 2,5-furanoate): A biobased polyester from 2,5-furan dicarboxylic acid. *RSC Adv.* **2015**, *5*, 74592–74604. [[CrossRef](#)]
128. Papageorgiou, D.G.; Guigo, N.; Tsanaktsis, V.; Exarhopoulos, S.; Bikiaris, D.N.; Sbirrazzuoli, N.; Papageorgiou, G.Z. Fast Crystallization and Melting Behavior of a Long-Spaced Aliphatic Furandicarboxylate Biobased Polyester, Poly(dodecylene 2,5-furanoate). *Ind. Eng. Chem. Res.* **2016**, *55*, 5315–5326. [[CrossRef](#)]
129. Bosq, N.; Guigo, N.; Sbirrazzuoli, N. Crystallization of polytetrafluoroethylene in a wide range of cooling rates: Nucleation and diffusion in the presence of nanosilica clusters. *Molecules* **2019**, *24*, 1797. [[CrossRef](#)]
130. Papageorgiou, G.Z.; Achilias, D.S.; Bikiaris, D.N. Crystallization Kinetics of Biodegradable Poly(butylene succinate) under Isothermal and Non-Isothermal Conditions. *Macromol. Chem. Phys.* **2007**, *208*, 1250–1264. [[CrossRef](#)]
131. Papageorgiou, G.Z.; Achilias, D.S.; Karayannidis, G.P. Estimation of thermal transitions in poly(ethylene naphthalate): Experiments and modeling using isoconversional methods. *Polymer* **2010**, *51*, 2565–2575. [[CrossRef](#)]
132. Stoclet, G.; Gobius du Sart, G.; Yeniad, B.; Lefebvre, J.M. Isothermal crystallization and structural characterization of poly(ethylene-2,5-furanoate). *Polymer* **2015**, *72*, 165–176. [[CrossRef](#)]
133. Tsanaktsis, V.; Papageorgiou, D.G.; Exarhopoulos, S.; Bikiaris, D.N.; Papageorgiou, G.Z. Crystallization and Polymorphism of Poly(ethylene furanoate). *Cryst. Growth Des.* **2015**, *15*, 5505–5512. [[CrossRef](#)]
134. Guigo, N.; van Berkel, J.; de Jong, E.; Sbirrazzuoli, N. Modelling the non-isothermal crystallization of polymers: Application to poly(ethylene 2,5-furandicarboxylate). *Thermochim. Acta* **2017**, *650*, 66–75. [[CrossRef](#)]
135. Sestak, J.; Berggren, G. Study of the kinetics of the mechanism of solid-state reactions at increasing temperatures. *Thermochim. Acta* **1971**, *3*, 1–12. [[CrossRef](#)]

136. van Berkel, J.G.; Guigo, N.; Kolstad, J.J.; Sipos, L.; Wang, B.; Dam, M.A.; Sbirrazzuoli, N. Isothermal crystallization kinetics of Poly (ethylene 2,5-furandicarboxylate). *Macromol. Mater. Eng.* **2015**, *300*, 466–474. [[CrossRef](#)]
137. Vyazovkin, S. A unified approach to kinetic processing of nonisothermal data. *Int. J. Chem. Kinet.* **1996**, *28*, 95–101. [[CrossRef](#)]
138. Burnham, A.K.; Dinh, L.N. A comparison of isoconversional and model-fitting approaches to kinetic parameter estimation and application predictions. *J. Therm. Anal. Calorim.* **2007**, *89*, 479–490. [[CrossRef](#)]
139. Serra, R.; Nomen, R.; Sempere, J. The non-parametric kinetics a new method for the kinetic study of thermoanalytical data. *J. Therm. Anal. Calorim.* **1998**, *52*, 933–943. [[CrossRef](#)]
140. Monzón, F.; Rovira, M.D.; Sempere, J.; Nomen, R. Determination of polymer crystallization kinetics with the NPK method. *J. Therm. Anal. Calorim.* **2022**, *147*, 10089–10093. [[CrossRef](#)]
141. Farjas, J.; Lopez-Olmedo, J.P.; Roura, P. Model-free isoconversional method applied to polymer crystallization governed by the Hoffman-Lauritzen kinetics. *Polymer* **2017**, *120*, 111–118. [[CrossRef](#)]
142. Arshad, M.A. A novel kinetic approach to crystallization mechanisms in polymers. *Polym. Eng. Sci.* **2021**, *61*, 1502–1517. [[CrossRef](#)]

Disclaimer/Publisher’s Note: The statements, opinions and data contained in all publications are solely those of the individual author(s) and contributor(s) and not of MDPI and/or the editor(s). MDPI and/or the editor(s) disclaim responsibility for any injury to people or property resulting from any ideas, methods, instructions or products referred to in the content.